Inorg. Chem. **2008**, *47*, 4095−4108

New Fe_4, Fe_6, and Fe_8 Clusters of Iron(III) from the Use of 2-Pyridyl Alcohols: Structural, Magnetic, and Computational Characterization

Taketo Taguchi,[†] Theocharis C. Stamatatos,[†] Khalil A. Abboud,[†] Candace M. Jones,[‡] Katye M. Poole,[‡] Ted A. O'Brien,[‡] and George Christou*[,†]

Department of Chemistry, University of Florida, Gainesville, Florida 32611, and Department of Chemistry and Chemical Biology, Indiana University−Purdue University Indianapolis, Indianapolis, Indiana 46202-3274

Received September 6, 2007

The syntheses, crystal structures, magnetochemical characterization, and theoretical calculations are reported for three new iron clusters $[Fe_6O_2(NO_3)_4(hmp)_8(H_2O)_2](NO_3)_2$ (**1**), $[Fe_4(N_3)_6(hmp)_6]$ (**2**), and $[Fe_8O_3(OMe)(pdm)_4(pdmH)_4(MeOH)_2](ClO_4)_5$ (**3**) (hmpH = 2-(hydroxymethyl)pyridine; $pdmH_2$ = 2,6-pyridinedimethanol). The reaction of hmpH with iron(III) sources such as $Fe(NO_3)_3 \cdot 9H_2O$ in the presence of NEt_3 gave **1**, whereas **2** was obtained from a similar reaction by adding an excess of NaN_3. Complex **3** was obtained in good yield from the reaction of $pdmH_2$ with $Fe(ClO_4)_3 \cdot 6H_2O$ in MeOH in the presence of an organic base. The complexes all possess extremely rare or novel core topologies. The core of **1** comprises two oxide-centered $[Fe_3(\mu_3\text{-}O)]^{7+}$ triangular units linked together at two of their apexes by two sets of alkoxide arms of hmp^- ligands. Complex **2** contains a zigzag array of four Fe^{III} atoms within an $[Fe_4(\mu\text{-}OR)_6]^{6+}$ core, with the azide groups all bound terminally. Finally, complex **3** contains a central $[Fe_4(\mu_4\text{-}O)]^{10+}$ tetrahedron linked to two oxide-centered $[Fe_3(\mu_3\text{-}O)]^{7+}$ triangular units. Variable-temperature, solid-state dc and ac magnetization studies were carried out on complexes **1**−**3** in the 5.0–300 K range. Fitting of the obtained magnetization versus field (*H*) and temperature (*T*) data by matrix diagonalization and including only axial anisotropy (zero-field splitting, ZFS) established that **1** possesses an $S = 3$ ground-state spin, with $g = 2.08$, and $D = -0.44$ cm^{-1}. The magnetic susceptibility data for **2** up to 300 K were fit by matrix diagonalization and gave $J_1 = -9.2$ cm^{-1}, $J_2 = -12.5$ cm^{-1}, and $g = 2.079$, where J_1 and J_2 are the outer and middle nearest-neighbor exchange interactions, respectively. Thus, the interactions between the Fe^{III} centers are all antiferromagnetic, giving an $S = 0$ ground state for **2**. Similarly, complex **3** was found to have an $S = 0$ ground state. Theoretically computed values of the exchange constants in **2** were obtained with DFT calculations and the ZILSH method and were in good agreement with the values obtained from the experimental data. Exchange constants obtained with ZILSH for **3** successfully rationalized the experimental $S = 0$ ground state. The combined work demonstrates the ligating flexibility of pyridyl-alcohol chelates and their usefulness in the synthesis of new polynuclear Fe_x clusters without requiring the copresence of carboxylate ligands.

Introduction

The last two decades have witnessed an explosive growth in the interest in polynuclear iron(III) compounds with primarily oxygen-based ligation. This has been mainly due to their relevance to two fields, bioinorganic chemistry and molecular magnetism, as well as the intrinsic architectural beauty and aesthetically pleasing structures they possess. Iron−oxo centers are found in several non-heme metalloproteins. Hemerythrin, ribonucleotide reductase, and methane monooxygenase are examples of enzymes with diiron metallosites,[1] whereas the protein ferritin, responsible for iron storage, can accommodate up to ∼4500 iron ions in an iron/oxide/hydroxide core.[2] A number of polynuclear iron complexes have thus been synthesized and studied as possible

* Author to whom correspondence should be addressed. E-mail: christou@chem.ufl.edu.
† University of Florida.
‡ IUPUI.

(1) (a) Kurtz, D. M. *Chem. Rev.* **1990**, *90*, 585. (b) Lippard, S. J. *Angew. Chem., Int. Ed. Engl.* **1988**, *27*, 344. (c) Toftlund, H.; Murray, K. S.; Zwack, P. R.; Taylor, L. F.; Anderson, O. P. *J. Chem. Soc., Chem. Commun.* **1986**, 191.

10.1021/ic701756p CCC: $40.75
Published on Web 04/24/2008

models for ferritin to gain insights into the biomineralization process involved in the formation of its metal core.[3] In the area of magnetism, high-spin iron(III) ions have a relatively large number of unpaired electrons (d^5, $S = {}^5/_2$) and normally undergo strong, antiferromagnetic exchange interactions. With high enough Fe_x nuclearities and appropriate topologies, these compounds can sometimes possess large ground-state spin (S) values and can even occasionally function as single-molecule magnets (SMMs).[4] The latter are molecules that display slow magnetization relaxation rates and which, below a certain (blocking) temperature (T_B), can function as single-domain magnetic particles of nanoscale dimensions.[5] Such SMMs thus represent a molecular, "bottom-up" approach to nanomagnetism.[5a]

Although exchange interactions between Fe^{III} centers are essentially always antiferromagnetic, certain Fe_x topologies can nevertheless result in large spin ground states because of spin frustration effects. Spin frustration is defined here in its general sense as the occurrence of competing exchange interactions of comparable magnitude that prevent (frustrate) the preferred spin alignments.[6] For example, in certain topologies the spins of two antiferromagnetically coupled metal ions (or other spin carriers) may be forced into a parallel alignment by other, stronger interactions; thus, the intrinsic preference of the spins to align antiparallel is frustrated. A sufficient quantity and distribution of frustrated exchange pathways in some Fe_x topologies can lead to the significantly large values of the total molecular spin mentioned above, even when all the pairwise Fe_2 exchange interactions are antiferromagnetic. Thus, we continue to have a great interest in rationalizing and understanding the exchange interactions and resulting ground state S of polynuclear Fe^{III} molecules.

For the above reasons, we continue to seek synthetic methods to new Fe_x complexes, and one approach that has proven successful is the use of alcohol-containing chelates. On deprotonation, these will provide alkoxide groups, which

Scheme 1

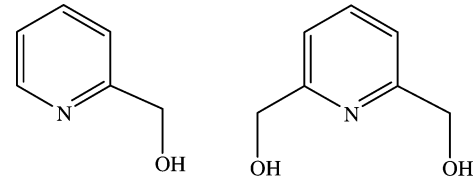

hmpH **pdmH$_2$**

are excellent bridging units that can foster formation of high nuclearity products.[7] We have a particular fondness for pyridyl alcohols (Scheme 1) which have proved to be versatile chelating and bridging groups that have yielded several polynuclear 3d metal clusters with large S values[8] and SMM behavior.[9] However, in Fe^{III} chemistry there has been only very limited use of hmpH, mostly by our own group in Fe_6[6a] and Fe_8[10] chemistry, and none for pdmH$_2$ except our heterometallic $[Fe_2M_2Cl_4(pdmH)_6]Cl_2$ ($M^{III} = Y$, Ho) complexes.[11] Even for the previously reported Fe^{III} clusters with pyridyl-alkoxide groups, the majority also contain carboxylate groups as a result of the use of triangular $[Fe_3O(O_2CR)_6(L)_3]^+$ compounds as reagents, a common strategy in both Fe^{III} [12] and Mn^{III} [13] chemistry. Carboxylates (RCO_2^-) are also excellent bridging groups in Fe^{III} chem-

(2) (a) Theil, E. C. *Annu. Rev. Biochem.* **1987**, *57*, 289. (b) Xu, B.; Chasteen, N. D. *J. Biol. Chem.* **1991**, *266*, 19965. (c) Bertini, I.; Gray, H. B.; Lippard, S. J.; Valentine, J. S. *Bioinorganic Chemistry*; University Science Books: Mill Valley, CA, 1994. (d) Powell, A. K. In *Comprehensive Coordination Chemistry II*; Mc Cleverty, J. A., Meyer, T. J., Eds.; Elsevier: Amsterdam, 2004; Vol. *8*, pp 169–194. (e) Theil, E. C.; Matzapetakis, M.; Liu, X. *J. Biol. Inorg. Chem.* **2006**, *11*, 803.

(3) (a) Taft, K. L.; Papaefthymiou, G. S.; Lippard, S. J. *Science* **1993**, *259*, 1302. (b) Gorun, S. M.; Papaefthymiou, G. S.; Frankel, R. B.; Lippard, S. J. *J. Am. Chem. Soc.* **1987**, *109*, 4244. (c) Powell, A. K. *Struct. Bonding (Berlin)* **1997**, *88*, 1.

(4) (a) Christou, G.; Gatteschi, D.; Hendrickson, D. N.; Sessoli, R. *MRS Bull.* **2000**, *25*, 66. (b) Gatteschi, D.; Sessoli, R. *Angew. Chem., Int. Ed.* **2003**, *42*, 268. (c) Bircher, R.; Chaboussant, G.; Dobe, C.; Güdel, H. U.; Ochsenbein, S. I.; Sieber, A.; Waldmann, O. *Adv. Funct. Mater.* **2006**, *16*, 209.

(5) (a) For recent reviews, see: Christou, G. *Polyhedron* **2005**, *24*, 2065. (b) Aromi, G.; Brechin, E. K. *Struct. Bonding (Berlin)* **2006**, *122*, 1.

(6) (a) O'Brien, T. O.; Taguchi, T; Stamatatos, T. C.; Christou, G. To be submitted. (b) McCusker, J. K.; Vincent, J. B.; Schmitt, E. A.; Mino, M. L.; Shin, K.; Coggin, D. K.; Hagen, P. M.; Huffman, J. C.; Christou, G.; Hendrickson, D. N. *J. Am. Chem. Soc.* **1991**, *113*, 3012. (c) Libby, E.; McCusker, J. K.; Schmitt, E. A.; Folting, K.; Hendrickson, D. N.; Christou, G. *Inorg. Chem.* **1991**, *31*, 3486. (d) Khan, O. *Chem. Phys. Lett.* **1997**, *265*, 109.

(7) (a) For some representative references, see: Jones, L. F.; Brechin, E. K.; Collison, D.; Helliwell, M.; Mallah, T.; Piligkos, S.; Rajaraman, G.; Wernsdorfer, W. *Inorg. Chem.* **2003**, *42*, 6601. (b) Jones, L. F.; Batsanov, A.; Brechin, E. K.; Collison, D.; Helliwell, M.; Mallah, T.; McInnes, E. J. L.; Piligkos, S. *Angew. Chem., Int. Ed.* **2002**, *41*, 4318. (c) Saalfrank, R. W.; Bernt, I.; Uller, E.; Hampel, F. *Angew. Chem., Int. Ed.* **1997**, *36*, 2482. (d) Goodwin, J. C.; Sessoli, R.; Gatteschi, D.; Wernsdorfer, W.; Powell, A. K.; Heath, S. L. *Dalton Trans.* **2000**, *12*, 1835.

(8) (a) Stamatatos, Th. C.; Abboud, K. A.; Wernsdorfer, W.; Christou, G. *Angew. Chem., Int. Ed.* **2006**, *45*, 4134. (b) Harden, N. C.; Bolcar, M. A.; Wernsdorfer, W.; Abboud, K. A.; Streib, W. E.; Christou, G. *Inorg. Chem.* 2003, *42*, 7067.

(9) (a) Murugesu, M.; Habrych, M.; Wernsdorfer, W.; Abboud, K. A.; Christou, G. *J. Am. Chem. Soc.* **2004**, *126*, 4766. (b) Stamatatos, Th. C.; Abboud, K. A.; Wernsdorfer, W.; Christou, G. *Angew. Chem., Int. Ed.* **2007**, *46*, 884. (c) Yoo, J.; Brechin, E. K.; Yamaguchi, A.; Nakano, M.; Huffman, J. C.; Maniero, A. L.; Brunel, L.- C.; Awaga, K.; Ishimoto, H.; Christou, G.; Hendrickson, D. N. *Inorg. Chem.* **2000**, *39*, 3615. (d) Boskovic, C.; Wernsdorfer, W.; Folting, K.; Huffman, J. C.; Hendrickson, D. N.; Christou, G. *Inorg. Chem.* **2002**, *41*, 5107. (e) Murugesu, M.; Wernsdorfer, W.; Abboud, K. A.; Christou, G. *Polyhedron* **2005**, *24*, 2894. (f) Yang, E.- C.; Harden, N.; Wernsdorfer, W.; Zakharov, L.; Brechin, E. K.; Rheingold, A. L.; Christou, G.; Hendrickson, D. N. *Polyhedron* **2003**, *22*, 1857. (g) Yang, E -C.; Wernsdorfer, W.; Hill, S.; Edwards, R. S.; Nakano, M.; Maccagnano, S.; Zakharov, L. N.; Rheingold, A. L.; Christou, G.; Hendrickson, D. N. *Polyhedron* **2003**, *22*, 1727. (h) Yang, E.- C.; Hendrickson, D. N.; Wernsdorfer, W.; Nakano, M.; Zakharov, L. N.; Sommer, R. D.; Rheingold, A. L.; Ledezma-Gairraud, M.; Christou, G. *J. Appl. Phys.* **2002**, *91*, 7382.

(10) Brechin, E. K.; Knapp, M. J.; Huffman, J. C.; Hendrickson, D. N.; Christou, G. *Inorg. Chim. Acta* **2000**, *297*, 389.

(11) Murugesu, M.; Mishra, A.; Wernsdorfer, W.; Abboud, K. A.; Christou, G. *Polyhedron* **2006**, *25*, 613.

(12) (a) Ammala, P.; Cashion, J. D.; Kepert, C. M.; Moubaraki, M.; Murray, K. S.; Spiccia, L.; West, B. O. *Angew. Chem., Int. Ed.* **2000**, *39*, 1688. (b) Murugesu, M.; Abboud, K. A.; Christou, G. *Polyhedron* **2004**, *23*, 2779. (c) Taft, K. L.; Lippard, S. J. *J. Am. Chem. Soc.* **1990**, *112*, 9629. (d) Benelli, C.; Parsons, S.; Solan, G. A.; Winpenny, R. E. P. *Angew. Chem., Int. Ed.* **1996**, *35*, 1825. (e) Bagai, R.; Datta, S.; Betancur-Rodriguez, A.; Abboud, K. A.; Hill, S.; Christou, G. *Inorg. Chem.* **2007**, *46*, 4535. (f) Bagai, R.; Abboud, K. A.; Christou, G. *Inorg. Chem.* **2007**, *46*, 5567.

(13) For a recent review, see: Brechin, E. K. *Chem. Commun.* **2005**, 5141.

istry.[14] In the present paper, we report some results from a recent investigation of non-carboxylate Fe^{III} cluster chemistry, which have led to new Fe_4, Fe_6, and Fe_8 products. We describe the syntheses, structures, and magnetochemical characterization of these complexes, as well as theoretical rationalization of the experimental observations.

Experimental Section

Syntheses. All manipulations were performed under aerobic conditions using chemicals and solvents as received unless otherwise stated.

Safety note! *Perchlorate and azide salts are potentially explosive; such compounds should be synthesized and used in small quantities and treated with utmost care at all times.*

$[Fe_6O_2(NO_3)_4(hmp)_8(H_2O)_2](NO_3)_2$ (1). To a stirred solution of hmpH (0.29 mL, 3.0 mmol) and NEt_3 (0.14 mL, 1.0 mmol) in MeCN (30 mL) was added solid $Fe(NO_3)_3 \cdot 9H_2O$ (0.40 g, 1.0 mmol). The resulting brown solution was stirred for 1 h and filtered, and the filtrate was layered with Et_2O (30 mL). After 2 days, large brown crystals of **1**·6MeCN were collected by filtration, washed with cold MeCN (2 × 5 mL) and Et_2O (2 × 5 mL), and dried under vacuum; the yield was ∼60%. Anal. Calcd for **1** (solvent-free): C, 35.15; H, 3.20; N, 11.96. Found: C, 35.03; H, 3.05; N, 11.68. Selected IR data (cm^{-1}): 3418 (mb), 1608 (m), 1570 (w), 1483 (w), 1439 (m), 1383 (s), 1285 (m), 1221 (w), 1156 (w), 1075 (m), 1049 (m), 1022 (w), 826 (w), 763 (m), 719 (m), 677 (m), 647 (m), 530 (m), 459 (w), 412 (w).

$[Fe_4(N_3)_6(hmp)_6]$ (2). To a stirred solution of hmpH (0.29 mL, 3.0 mmol) and NEt_3 (0.14 mL, 1.0 mmol) in a solvent mixture comprised of MeCN/MeOH (30 mL, 5:1 v/v) was added solid $Fe(NO_3)_3 \cdot 9H_2O$ (0.40 g, 1.0 mmol). The resulting brown solution was stirred for 1 h, during which time solid NaN_3 (0.20 g, 3.0 mmol) was added in small portions. The resulting dark red solution was stirred for a further 3 h and filtered, and the filtrate was layered with Et_2O (30 mL). After 6 days, dark red crystals of **2**·2MeOH were collected by filtration, washed with cold MeCN (2 × 5 mL) and Et_2O (2 × 5 mL), and dried under vacuum; the yield was ∼50%. Anal. Calcd for **2** (solvent-free): C, 38.46; H, 3.23; N, 29.90. Found: C, 38.73; H, 3.07; N, 29.49. Selected IR data (cm^{-1}): 3419 (mb), 2077 (s), 2052 (s), 1607 (m), 1568 (w), 1482 (m), 1433 (m), 1355 (m), 1287 (m), 1220 (w), 1154 (w), 1085 (m), 1060 (m), 1047 (m), 821 (w), 764 (m), 721 (m), 667 (m), 647 (m), 513 (m), 474 (w), 420 (m).

$[Fe_8O_3(OMe)(pdm)_4(pdmH)_4(MeOH)_2](ClO_4)_5$ (3). To a stirred solution of $pdmH_2$ (0.14 g, 1.0 mmol) and NEt_3 (0.14 mL, 1.0 mmol) in MeOH (30 mL) was added solid $Fe(ClO_4)_3 \cdot 6H_2O$ (0.46 g, 1.0 mmol). The resulting brown solution was stirred for 1 h and filtered, and the filtrate was layered with Et_2O (30 mL). After 2 days, large brown crystals of **3**·7MeOH were collected by filtration, washed with cold MeOH (2 × 5 mL) and Et_2O (2 × 5 mL), and dried under vacuum; the yield was ∼50%. Anal. Calcd for **3** (solvent-free): C, 32.38; H, 3.27; N, 5.12. Found: C, 32.53; H, 3.09; N, 5.09. Selected IR data (cm^{-1}): 3428 (mb), 1606 (m), 1582 (w), 1469 (w), 1438 (w), 1345 (w), 1265 (w), 1218 (w), 1144 (s), 1118 (s), 1089 (s), 786 (m), 720 (m), 676 (m), 628 (m), 592 (m), 510 (m), 467 (w), 430 (w).

X-ray Crystallography. Data were collected on a Siemens SMART PLATFORM equipped with a CCD area detector and a graphite monochromator utilizing Mo Kα radiation ($\lambda = 0.71073$ Å). Suitable crystals of **1**·6MeCN, **2**·2MeOH, and **3**·7MeOH were attached to glass fibers using silicone greaseand transferred to a goniostat where they were cooled to 173 K for data collection. An initial search of reciprocal space revealed a triclinic cell for **1**·6MeCN and **3**·7MeOH, and a monoclinic cell for **2**·2MeOH; the choices of space groups $P\bar{1}$ (for **1**·6MeCN and **3**·7MeOH) and $P2_1/c$ (for **2**·2MeOH) were confirmed by the subsequent solution and refinement of the structures. Cell parameters were refined using up to 8192 reflections. A full sphere of data (1850 frames) was collected using the ω-scan method (0.3° frame width). The first 50 frames were remeasured at the end of data collection to monitor instrument and crystal stability (maximum correction on I was <1%). Absorption corrections by integration were applied based on measured indexed crystal faces. The structures were solved by direct methods in SHELXTL6,[15] and refined on F^2 using full-matrix least-squares. The non-H atoms were treated anisotropically, whereas the H atoms were placed in calculated, ideal positions and refined as riding on their respective C atoms. Unit cell parameters and structure solution and refinement data are listed in Table 1.

Table 1. Crystallographic Data for **1**·6MeCN, **2**·2MeOH, and **3**·7MeOH

parameter	**1**	**2**	**3**
formula[a]	$C_{60}H_{70}N_{20}O_{30}Fe_6$	$C_{38}H_{44}N_{24}O_8Fe_4$	$C_{66}H_{99}N_8O_{42}Cl_5Fe_8$
fw, g mol^{-1} [a]	1886.46	1188.37	2300.58
crystal system	triclinic	monoclinic	triclinic
space group	$P\bar{1}$	$P2_1/c$	$P\bar{1}$
a, Å	11.8677(8)	13.6914(10)	13.6178(14)
b, Å	13.0369(9)	14.1350(11)	18.6824(19)
c, Å	13.9403(10)	13.6611(10)	19.069(2)
α, deg	64.628(2)	90	78.547(2)
β, deg	82.289(2)	104.942(1)	76.319(2)
γ, deg	73.042(2)	90	87.39(2)
V, Å^3	1863.9(2)	2554.4(3)	4619.9(8)
Z	1	2	2
T, °C	173(2)	173(2)	173(2)
radiation, Å[b]	0.71073	0.71073	0.71073
ρ_{calc}, g cm^{-3}	1.681	1.545	1.654
μ, mm^{-1}	1.236	1.187	1.457
R1[c,d]	0.0411	0.0482	0.0702
wR2[e]	0.1005	0.1156	0.1666

[a] Including solvate molecules. [b] Graphite monochromator. [c] $I > 2\sigma(I)$. [d] $R1 = \sum(||F_o| - |F_c||)/\sum F_o|$. [e] $wR2 = [\sum[w(F_o^2 - F_c^2)^2]/\sum[w(F_o^2)^2]]^{1/2}$, $w = 1/[\sigma^2(F_o^2) + [(ap)^2 + bp]$, where $p = [\max(F_o^2, 0) + 2F_c^2]/3$.

For **1**·6MeCN, the asymmetric unit consists of half of the Fe_6 cation, one NO_3^- anion, and three disordered MeCN molecules of crystallization. The latter could not be modeled properly; thus the program SQUEEZE,[16] a part of the PLATON package of crystallographic software, was used to calculate the solvent disorder area and remove its contribution to the overall intensity data. One coordinated NO_3^- (monodentate) has all three O atoms disordered while the second (also monodentate) has only two O atoms disordered, with the third O being common to both parts. A total of 447 parameters were included in the structure refinement using 8212 reflections with $I > 2\sigma(I)$ to yield R1 and wR2 of 4.11 and 10.05%, respectively.

For **2**·2MeOH, the asymmetric unit consists of half of the Fe_4 cluster and a MeOH molecule of crystallization disordered near an inversion center. The azide ligand consisting of atoms N10−N11−N12 is disordered, and the N11−N12 segment was refined in two parts with their site occupation factors dependently refined. A total of

(14) For a review, see: Papaefstathiou, G. S.; Perlepes, S. P. *Comments Inorg. Chem.* **2002**, *23*, 249.

(15) *SHELXTL6*; Bruker-AXS, Madison, WI, 2000.

(16) Van der Sluis, P.; Spek, A. L. *Acta Crystallogr., Sect. A: Found. Crystallogr.* **1990**, *A46*, 194.

332 parameters were included in the structure refinement using 5769 reflections with $I > 2\sigma(I)$ to yield R1 and wR2 of 4.82 and 11.56%, respectively.

For **3**·7MeOH, the asymmetric unit consists of the complete Fe_8 cluster, five ClO_4^- anions, and seven MeOH molecules of crystallization. A total of 1225 parameters were included in the structure refinement using 30354 reflections with $I > 2\sigma(I)$ to yield R1 and wR2 of 7.02 and 16.66%, respectively.

Physical Measurements. Infrared spectra were recorded in the solid state (KBr pellets) on a Nicolet Nexus 670 FTIR spectrometer in the 400–4000 cm^{-1} range. Elemental analyses (C, H, and N) were performed by the in-house facilities of the University of Florida Chemistry Department. Variable-temperature dc and ac magnetic susceptibility data were collected at the University of Florida using a Quantum Design MPMS-XL SQUID susceptometer equipped with a 7 T magnet and operating in the 1.8–300 K range. Samples were embedded in solid eicosane to prevent torquing. Magnetization versus field and temperature data were fit using the program MAGNET.[17a] Pascal's constants were used to estimate the diamagnetic corrections, which were subtracted from the experimental susceptibilities to give the molar paramagnetic susceptibilities (χ_M). The exchange interactions in **2** were calculated using matrix diagonalization methods described elsewhere.[18]

Theoretical Calculations. Density functional theory (DFT) calculations and semiempirical molecular orbital calculations with the ZILSH[18,19] method were used to estimate the exchange constants for compound **2**. ZILSH calculations were also performed on the larger compound **3**. According to the ZILSH procedure, energies are obtained for unrestricted Hartree–Fock (UHF) wave functions with the INDO/S method of Zerner[20] for spin components in which the spins of certain metals are reversed relative to the others. Spin couplings $\langle \hat{S}_A \cdot \hat{S}_B \rangle^{UHF}$ (A, B label metal ions) appearing in the Heisenberg spin Hamiltonian are obtained with the local spin operator of Davidson.[21] The spin couplings are thus obtained directly from the unrestricted wave functions with the local spin operator rather than arbitrarily assigned values based on spin projection or appropriate for spin eigenfunctions rather than unrestricted single determinant wave functions. Using expectation values of the local spin operator has a sounder theoretical basis, incorporating covalent interactions and spin delocalization, as described in detail in ref 19. We have successfully used this method to model magnetic interactions in numerous complexes.[18,19,22],

Energies and spin couplings obtained as described above are assumed to follow an effective Heisenberg formula given in eq 1, where i labels the spin component and E_0 contains all spin-independent contributions to the energy. Given the energies and spin couplings for a sufficient number of components, multiple eq 1 can be solved simultaneously for E_0 and the exchange constants J_{AB}. A similar strategy is used for the DFT calculations; a detailed description of the procedure is given elsewhere.[23] In summary, energies are obtained for unrestricted Kohn–Sham determinants describing the various spin components. These energies are used in eq 1 with spin couplings computed from the corresponding ZILSH wave functions with the local spin operator to obtain estimates of the exchange constants. This procedure closely resembles that used for DFT and molecular orbital calculations by others,[21,23,24] except that spin couplings are arbitrarily assigned values based on spin projection or assuming spin eigenfunctions rather than unrestricted Kohn–Sham determinants in these other calculations. It has been shown that spin couplings computed from Kohn–Sham determinants and ZILSH unrestricted determinants are very similar, and we have successfully used these interchangeably in previous calculations.[23]

$$E_i = E_0 - 2\sum_{A<B} J_{AB}\langle \hat{S}_A \cdot \hat{S}_B \rangle^{UHF} \quad (1)$$

DFT calculations on **2** used the B3LYP functional[25] with the all-electron Dunning–Huzinaga double-ζ basis set for light atoms[26] and the Los Alamos effective core potential plus double-ζ valence basis set for iron atoms[27] (LANL2DZ). All DFT calculations were run to a self-consistent field (SCF) convergence of 10^{-8} au using the Gaussian03 program.[28] ZILSH SCF calculations on **2** and **3** were converged to machine precision (10^{-13} au). The ZILSH and DFT calculations also both provide the local spin density M_i for each metal ion, equal to the number of unpaired electrons associated with that ion.[19] This quantity indicates if the correct oxidation states and metal d electron configurations were obtained for the metal ions.

Given exchange constants obtained as just described, wave

(17) (a) Davidson, E. R. *MAGNET*; Indiana University, Bloomington, IN, 1999. (b) Davidson, E. R. *GRID* Indiana University, Bloomington, IN, 1999.

(18) Cañada-Vilalta, C.; O'Brien, T. A.; Brechin, E. K.; Pink, M.; Davidson, E. R.; Christou, G. *Inorg. Chem.* **2004**, *43*, 5505.

(19) O'Brien, T. A.; Davidson, E. R. *Int. J. Quantum Chem.* **2003**, *92*, 294.

(20) Zerner, M. C.; Loew, G. H.; Kirchner, R. F.; Mueller-Westerhoff, U. T. *J. Am. Chem. Soc.* **1980**, *102*, 589.

(21) Clark, A. E.; Davidson, E. R. *J. Chem. Phys.* **2001**, *115*, 7382.

(22) (a) Tasiopoulos, A. J.; O'Brien, T. A.; Abboud, K. A.; Chistou, G. *Angew. Chem., Int. Ed.* **2004**, *43*, 345. (b) Foguet-Albiol, D.; O'Brien, T. A.; Wernsdorfer, W.; Moulton, B.; Zaworotko, M. J.; Abboud, K. A.; Christou, G. *Angew. Chem., Int. Ed.* **2005**, *44*, 897. (c) Canada-Vilalta, C.; Streib, W. E.; Huffman, J. C.; O'Brien, T. A.; Davidson, E. R.; Christou, G. *Inorg. Chem.* **2004**, *43*, 101. (d) Tasiopoulos, A. J.; Milligan, P. L.; Abboud, K. A.; O'Brien, T. A.; Christou, G. *Inorg. Chem.* **2007**, *46*, 9678.

(23) Davidson, E. R.; Clark, A. E. *J. Phys. Chem. A* **2002**, *106*, 7456.

(24) (a) Zhao, X. G.; Richardson, W. H.; Chen, J. L.; Li, J.; Noodleman, L.; Tsai, H. L.; Hendrickson, D. N. *Inorg. Chem.* **1997**, *36*, 1198. (b) Yamaguchi, K.; Fukui, H.; Fueno, T. *Chem. Lett.* **1986**, 625. (c) Yamaguchi, K. *Chem. Phys. Lett.* **1975**, *33*, 330. (d) Soda, T.; Kitagawa, Y.; Onishi, T.; Takano, Y.; Nagao, H.; Yoshioka, Y.; Yamaguchi, K. *Chem. Phys. Lett.* **2000**, *319*, 223. (e) Ruiz, E.; Alvarez, S.; Cano, J.; Polo, V. *J. Chem. Phys.* **2005**, 164110. (f) Rajaraman, G.; Cano, J.; Brechin, E. K.; McInnes, E. J. L. *Chem. Commun.* **2004**, 1476. (g) Noodleman, L.; Norman, J. G. *J. Chem. Phys.* **1979**, *70*, 4903. (h) Noodleman, L.; Davidson, E. R. *Chem. Phys.* **1986**, *109*, 131. (i) Noodleman, L. *J. Chem. Phys.* **1981**, *74*, 5737. (j) Hay, P. J.; Thibeault, J. C.; Hoffmann, R. *J. Am. Chem. Soc.* **1975**, *97*, 4884. (k) Estiu, G. L.; Cory, M. G.; Zerner, M. C. *J. Phys. Chem. A* **2000**, *104*, 233. (l) Cory, M. G.; Stavrev, K. K.; Zerner, M. C. *Int. J. Quantum Chem.* **1997**, *63*, 781. (m) Cauchy, T.; Ruiz, E.; Alvarez, S. *Physica B* **2006**, *384*, 116. (n) Cano, J.; Costa, R.; Alvarez, S.; Ruiz, E. *J. Chem. Theory Comput.* **2007**, *3*, 782.

(25) Becke, A. D. *J. Chem. Phys.* **1993**, *98*, 5648.

(26) Dunning, T. H.; Hay, P. J. In *Modern Theoretical Chemistry*; Plenum: New York, 1976; pp 1–28.

(27) Hay, P. J.; Wadt, W. R. *J. Chem. Phys.* **1985**, *82*, 270.

(28) Frisch, M. J.; Trucks, G. W.; Schlegel, H. B.; Scuseria, G. E.; Robb, M. A.; Cheeseman, J. R.; Montgomery, J. A., Jr.; Vreven, T.; Kudin, K. N.; Burant, J. C.; Millam, J. M.; Iyengar, S. S.; Tomasi, J.; Barone, V.; Mennucci, B.; Cossi, M.; Scalmani, G.; Rega, N.; Petersson, G. A.; Nakatsuji, H.; Hada, M.; Ehara, M.; Toyota, K.; Fukuda, R.; Hasegawa, J.; Ishida, M.; Nakajima, T.; Honda, Y.; Kitao, O.; Nakai, H.; Klene, M.; Li, X.; Knox, J. E.; Hratchian, H. P.; Cross, J. B.; Adamo, C.; Jaramillo, J.; Gomperts, R.; Stratman, R. E.; Yazyev, O.; Austin, A. J.; Cammi, R.; Pomell, C.; Ochterski, J. W.; Ayala, P. Y.; Morokuma, K.; Voth, G. A.; Salvador, P.; Dannenberg, J. J.; Zakrzewski, V. G.; Dapprich, S.; Daniels, A. D.; Strain, M. C.; Farkas, O.; Malick, D. K.; Rabuck, A. D.; Raghavachari, K.; Foresman, J. B.; Ortiz, J. V.; Cui, Q.; Baboul, A. G.; Clifford, S.; Cioslowski, J.; Stefanov, B. B.; Liu, G.; Liashenko, A.; Piskorz, P.; Komaromi, I.; Martin, R. L.; Fox, D. J.; Keith, T.; Al-Laham, M. A.; Peng, C. Y.; Nanayakkara, A.; Challacombe, M.; Gill, P. M. W.; Johnson, B.; Chen, W.; Wong, M. W.; Gonzalez, C.; Pople, J. A. *Gaussian03, Revision B.05*, Gaussian, Inc.: Pittsburgh, PA, 2003.

functions and energies for the spin eigenstates of a complex can be found by substituting the exchange constants into the Heisenberg spin Hamiltonian. The operator is then diagonalized in a basis of spin components $\varphi_i = |m_1\ m_2 \ldots m_N\rangle_i$, where m_A is a formal value of the local z component of spin of metal "A" ($m_A = {}^5/_2, {}^3/_2, \ldots, -{}^5/_2$ for high-spin d^5 Fe^{3+} ions). The resulting spin eigenstate wave functions are then linear combinations of these components (eq 2), where the expansion runs over components

$$|\psi_S\rangle = \sum_i C_i \varphi_i \qquad (2)$$

for which the local z components of spin add to the total spin S of the state. In this work the diagonalization was carried out with the Davidson algorithm,[29,30,31] which provides the energy and wave function for the lowest energy state of each spin.

One important quantity that can be calculated from the wave functions is the spin coupling $\langle \hat{S}_A \cdot \hat{S}_B \rangle$ for each pair of metal ions. These values are useful for identifying exchange pathways that are spin frustrated.[30,31] The spin coupling indicates the actual alignment of z components m_A and m_B in the state, while the exchange constant J_{AB} indicates the preferred alignment. Any pathway with $\langle \hat{S}_A \cdot \hat{S}_B \rangle$ and J_{AB} of different signs is thus frustrated under the $-2J$ convention. This is used to describe the spin interactions in the ground state of **3** (vide infra).

Results and Discussion

Syntheses. As stated earlier, the present study arose as part of our investigation of the reactions of hmpH and $pdmH_2$ with Fe^{III} sources in the absence of carboxylate groups. We have in some cases also added a source of azides, which are also excellent bridging ligands and can foster the formation of high nuclearity products.[32,33]

Various reactions have been systematically explored with differing reagent ratios, reaction solvents, and other conditions. The reaction of $Fe(NO_3)_3 \cdot 9H_2O$ with hmpH and NEt_3 in a 1:3:1 molar ratio in MeCN gave a brown solution and the subsequent isolation of well-formed brown crystals of $[Fe_6O_2(NO_3)_4(hmp)_8(H_2O)_2](NO_3)_2 \cdot 6MeCN$ (**1**·6MeCN) in high yields (~50%). The formation of **1** is summarized in eq 3. Note that the NEt_3 has the role of proton acceptor to facilitate both the deprotonation of the hmpH groups and H_2O molecules as a source of the bridging O^{2-} ions; although the excess of hmpH employed could in principle also carry out these roles, the yield of complex **1** was only ~2% in the absence of NEt_3. However, when more than 1 equiv of NEt_3 was used, insoluble amorphous precipitates that were probably polymeric were rapidly formed. On the other hand, an increase in the amount of hmpH to 5 equiv (or more) did not give **1** but the similar product $[Fe_6O_2(hmp)_{10}(H_2O)_2](NO_3)_4$ in high yields (>50%).[6a] This is structurally similar to **1** except that the four terminal NO_3^- groups have been replaced by two chelating hmp^- groups. Complex **1** was also obtained using other reaction solvents (i.e., MeOH, CH_2Cl_2), but the yields were appreciably lower and the crystalline precipitate was found to be contaminated with some other solid products. Other reactions with higher Fe^{3+}/hmpH ratios also gave compound **1**.

$$6Fe^{3+} + 8hmpH + 12NEt_3 + 4NO_3^- + 4H_2O \rightarrow [Fe_6O_2(NO_3)_4(hmp)_8(H_2O)_2]^{2+} + 12NHEt_3^+ \quad (3)$$

The addition of 3 equiv of NaN_3 to the reaction mixture that yields **1**, but in a MeCN/MeOH solvent mixture to aid solubility, gave a deep red solution and subsequent isolation of $[Fe_4(N_3)_6(hmp)_6] \cdot 2MeOH$ (**2**·2MeOH) in yields of ~50%. The formation of **2** is summarized in eq 4. The same product was also obtained using only MeCN as the reaction solvent, but longer reaction times were needed and the product was contaminated with white solids. Increasing the amount of sodium azide still gave complex **2**, but the reaction was not so clean and the yield was appreciably lower. With the identity of **2** established, we also tried several other Fe^{3+}/hmpH/NEt_3/N_3^- ratios, and particularly with a large excess of FeX_3 ($X = Cl^-, NO_3^-, ClO_4^-$), to see if higher nuclearity azide-containing products might be obtained, but in all cases complex **2** was the isolated product, in varying yields. As for **1**, the NEt_3 was again essential to obtain **2** in good yields and too much NEt_3 also again gave insoluble powders, which formed rapidly from the reaction solution.

$$4Fe^{3+} + 6hmpH + 6NEt_3 + 6N_3^- \rightarrow [Fe_4(N_3)_6(hmp)_6] + 6NHEt_3^+ \quad (4)$$

A number of reactions have also been investigated with $pdmH_2$. Treatment of an equimolar mixture of $Fe(ClO_4)_3 \cdot 6H_2O$, $pdmH_2$, and NEt_3 in MeOH gave a brown solution from which were subsequently isolated large brown crystals of $[Fe_8O_3(OMe)(pdm)_4(pdmH)_4(MeOH)_2](ClO_4)_5 \cdot 7MeOH$ (**3**·7MeOH) in ~50% yield. The formation of the cation of **3** is summarized in eq 5. The use of other alcohols such as EtOH and Pr^nOH, or a nonalcohol such as MeCN or CH_2Cl_2, as reaction solvent gave only insoluble, amorphous precipitates that we were not able to characterize further. An increase of the NEt_3:$pdmH_2$ ratio up to 3:1 gave comparable (or slightly increased) yields of complex **3** rather than a hoped for higher nuclearity product as a result of complete deprotonation of $pdmH^-$ groups. Further increase of the amount of NEt_3 led to amorphous, insoluble precipitates. Complex **3** was also obtained, but in lower yields (<30%), from reactions with Fe^{III}:pdmH ratios of 2:1, 3:1, and 1:2 in MeOH. Clearly, complex **3** is the preferred product of these reaction components under these conditions.

$$8Fe^{3+} + 8pdmH_2 + 19NEt_3 + 3H_2O + 3MeOH \rightarrow [Fe_8O_3(OMe)(pdm)_4(pdmH)_4(MeOH)_2]^{5+} + 19NHEt_3^+ \quad (5)$$

Description of Structures. The partially labeled structure of the cation of complex **1** is shown in Figure 1. Selected interatomic distances and angles are listed in Table 2. Complex **1** crystallizes in triclinic space group $P\bar{1}$ and displays crystallographic C_i symmetry. The structure comprises six Fe atoms in a chair conformation. This can be

(29) Davidson, E. R. *J. Comput. Phys.* **1975**, *17*, 87.
(30) Cañada-Vilalta, C.; O'Brien, T. A.; Pink, M.; Davidson, E. R.; Christou, G. *Inorg. Chem.* **2003**, *42*, 7819.
(31) O'Brien, T. A.; O'Callaghan, B. J. J. *Chem. Theory Comput.* **2007**, *3*, 1275.
(32) For a recent review on the coordination chemistry of azides, see: Escuer, A.; Aromi, G. *Eur. J. Inorg. Chem.* **2006**, 4721.
(33) Stamatatos, T. C. *PhD Thesis*, University of Patras, Greece, 2006.

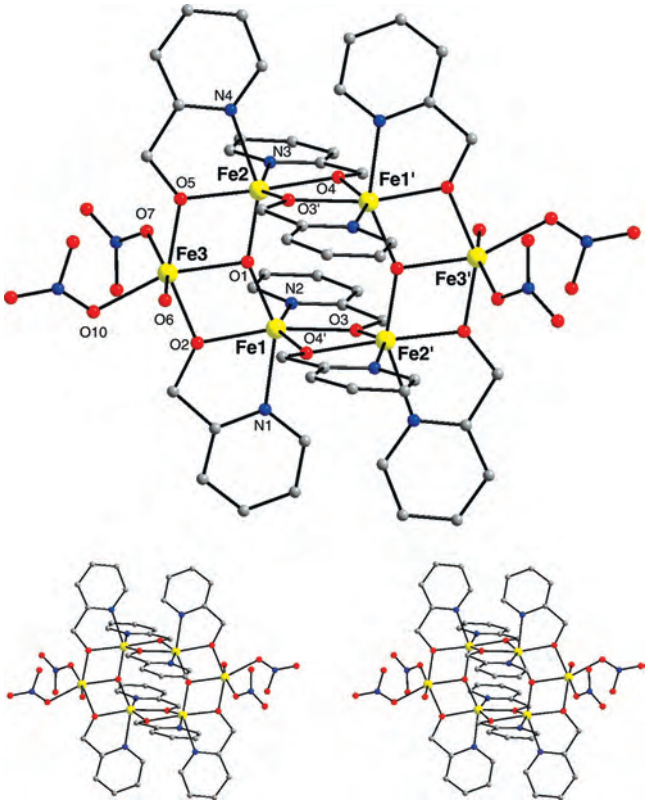

Figure 1. (Top) Labeled PovRay representation of the structure of **1**, with the hydrogen atoms omitted for clarity. (Bottom) A stereopair.

described as a central Fe_4 rectangle (Fe1, Fe1′, Fe2, Fe2′) with two additional Fe atoms (Fe3 and Fe3′) at two opposite ends and 1.544(2) Å above and below the central Fe_4 plane (Figure 2). However, a better description of the structure is as two triangular [$Fe_3(\mu_3\text{-}O^{2-})$] units joined together at two of their apexes; each connection, between Fe1/Fe2′ and Fe1′/Fe2, consists of two bridging hmp^- alkoxo groups. Each [$Fe_3(\mu_3\text{-}O^{2-})$] triangular unit is essentially isosceles (Fe1···Fe3 = 3.127(5) Å, Fe2···Fe3 = 3.095(3) Å, Fe1···Fe2 = 3.648(3) Å) and essentially planar (the oxide is only 0.004 Å from the Fe_3 plane), and the μ_3-oxide has Y-shaped geometry with the largest angle Fe1−O3−Fe2 being 149.1(1)°. The two equivalent sides of each isosceles triangle are bridged by an alkoxide O atom of a hmp^- group that chelates to a basal Fe atom. The ligation is completed by two monodentate NO_3^- groups on each apical Fe atom Fe3 and Fe3′, each of the latter also possessing a terminal H_2O ligand. All the Fe atoms are six-coordinate with distorted octahedral geometries. The distortions at the four central Fe atoms are particularly pronounced, with angles at cis and trans ligands ranging from 72.6(8) to 114.9(8)° and 147.5(8) to 173.3(8)°, respectively. The NO_3^- counterions are hydrogen bonded to the terminal water groups on Fe3 and Fe3′ (O6···O15 = 2.689(2) Å, O6···O14 = 2.672(2) Å) and serve to bridge separate Fe_6 molecules in the crystal.

There are several structural types of Fe^{III}_6 clusters already in the literature, differing in the Fe_6 topology. These have been conveniently referred to as (a) planar,[34] (b) twisted-boat,[35] (c) chairlike,[6a,36] (d) parallel triangles,[37] (e) octahedral,[38] (f) fused or extended butterflies,[39] (g) cyclic,[40] and (h) linked triangles.[41] As can be anticipated, these different Fe_6 topologies have led to a variety of ground-state spin S values among these complexes, spanning $S = 0$, 1, 3, and 5. There are two other Fe^{III}_6 complexes possessing a chairlike conformation, $[Fe_6O_2Cl_4(hmp)_8](ClO_4)_2$[36] and

Table 2. Selected Interatomic Distances (Å) and Angles (deg) for **1**·6MeCN, **2**·2MeOH, and **3**·7MeOH[a]

		1·6MeCN	
Fe(1)···Fe(2)	3.648(3)	Fe(2)···Fe(3)	3.095(3)
Fe(1)···Fe(3)	3.127(5)	Fe(1)···Fe(2′)	3.190(6)
Fe(1)−O(1)	1.890(2)	Fe(2)−O(5)	1.996(2)
Fe(1)−O(2)	1.997(2)	Fe(2)−N(3)	2.151(2)
Fe(1)−O(3)	2.010(2)	Fe(2)−N(4)	2.159(2)
Fe(1)−O(4′)	1.999(2)	Fe(3)−O(1)	2.018(2)
Fe(1)−N(1)	2.194(2)	Fe(3)−O(2)	1.996(2)
Fe(1)−N(2)	2.180(2)	Fe(3)−O(5)	1.992(2)
Fe(2)−O(1)	1.894(2)	Fe(3)−O(6)	2.034(2)
Fe(2)−O(3′)	1.975(2)	Fe(3)−O(7)	2.044(4)
Fe(2)−O(4)	2.005(2)	Fe(3)−O(10)	2.107(5)
Fe(1)−O(1)−Fe(2)	149.1(1)	Fe(1)−O(3)−Fe(2′)	106.4(8)
Fe(1)−O(1)−Fe(3)	106.2(9)	Fe(1)−O(4′)−Fe(2′)	105.7(8)
Fe(2)−O(1)−Fe(3)	104.5(8)	Fe(2)−O(5)−Fe(3)	101.8(8)
Fe(1)−O(2)−Fe(3)	103.1(8)		
		2·2MeOH	
Fe(1)···Fe(1′)	3.165(1)	Fe(2)···Fe(2′)	8.709(3)
Fe(1)···Fe(2)	3.170(1)	Fe(2)−O(1)	2.058(2)
Fe(1)−O(1)	1.954(2)	Fe(2)−O(3)	2.072(2)
Fe(1)−O(2)	1.997(2)	Fe(2)−N(3)	2.191(3)
Fe(1)−O(2′)	1.988(2)	Fe(2)−N(4)	2.012(3)
Fe(1)−O(3)	1.989(2)	Fe(2)−N(7)	1.988(3)
Fe(1)−N(1)	2.139(3)	Fe(2)−N(10)	2.016(3)
Fe(1)−N(2)	2.135(3)	Fe(1)−O(1)−Fe(2)	104.3(1)
Fe(1)−O(2)−Fe(1′)	105.2(1)	Fe(1)−O(3)−Fe(2)	102.6(9)
		3·7MeOH	
Fe(1)−O(1)	2.090(4)	Fe(5)−O(7)	2.034(4)
Fe(1)−O(2)	2.177(4)	Fe(5)−O(12)	2.078(4)
Fe(1)−O(3)	2.072(4)	Fe(5)−O(13)	2.145(5)
Fe(1)−O(9)	2.177(4)	Fe(5)−O(14)	2.074(5)
Fe(1)−O(21)	2.009(4)	Fe(5)−O(15)	1.973(4)
Fe(1)−O(22)	1.978(4)	Fe(5)−O(16)	2.160(5)
Fe(1)−N(1)	2.220(5)	Fe(5)−N(6)	2.240(5)
Fe(2)−O(3)	2.010(4)	Fe(6)−O(15)	1.920(4)
Fe(2)−O(4)	2.147(5)	Fe(6)−O(16)	2.006(4)
Fe(2)−O(5)	2.005(4)	Fe(6)−O(17)	2.000(4)
Fe(2)−O(6)	2.020(4)	Fe(6)−O(18)	1.998(4)
Fe(2)−O(22)	1.865(4)	Fe(6)−O(19)	2.096(4)
Fe(2)−N(2)	2.106(6)	Fe(6)−N(7)	2.051(6)
Fe(3)−O(6)	2.059(4)	Fe(7)−O(5)	2.011(4)
Fe(3)−O(7)	2.072(4)	Fe(7)−O(17)	2.033(4)
Fe(3)−O(8)	2.068(4)	Fe(7)−O(19)	1.958(4)
Fe(3)−O(10)	1.992(4)	Fe(7)−O(20)	2.053(4)
Fe(3)−O(19)	1.952(4)	Fe(7)−O(21)	2.088(4)
Fe(3)−N(3)	2.084(5)	Fe(7)−N(8)	2.060(5)
Fe(4)−O(10)	2.026(4)	Fe(8)−O(8)	2.003(4)
Fe(4)−O(11)	2.157(4)	Fe(8)−O(9)	2.015(4)
Fe(4)−O(12)	1.993(4)	Fe(8)−O(18)	1.948(4)
Fe(4)−O(15)	1.856(4)	Fe(8)−O(19)	2.089(4)
Fe(4)−O(20)	2.005(4)	Fe(8)−O(22)	1.915(4)
Fe(4)−N(5)	2.109(5)	Fe(8)−N(4)	2.080(5)
Fe(1)−O(3)−Fe(2)	100.3(2)	Fe(3)−O(19)−Fe(8)	99.7(2)
Fe(1)−O(9)−Fe(8)	95.3(2)	Fe(4)−O(12)−Fe(5)	100.4(2)
Fe(1)−O(21)−Fe(7)	126.3(2)	Fe(4)−O(15)−Fe(5)	109.5(2)
Fe(1)−O(22)−Fe(2)	109.2(2)	Fe(4)−O(15)−Fe(6)	139.4(2)
Fe(1)−O(22)−Fe(8)	105.6(2)	Fe(4)−O(20)−Fe(7)	118.3(2)
Fe(2)−O(5)−Fe(7)	117.1(2)	Fe(5)−O(15)−Fe(6)	105.3(2)
Fe(2)−O(6)−Fe(3)	118.1(2)	Fe(5)−O(16)−Fe(6)	95.9(2)
Fe(2)−O(22)−Fe(8)	138.1(2)	Fe(6)−O(17)−Fe(7)	99.3(2)
Fe(3)−O(7)−Fe(5)	125.2(2)	Fe(6)−O(18)−Fe(8)	106.4(2)
Fe(3)−O(8)−Fe(8)	98.8(2)	Fe(6)−O(19)−Fe(7)	98.5(2)
Fe(3)−O(10)−Fe(4)	117.0(2)	Fe(6)−O(19)−Fe(8)	98.1(2)
Fe(3)−O(19)−Fe(6)	112.5(2)		

[a] Primed and unprimed atoms are related by the inversion center.

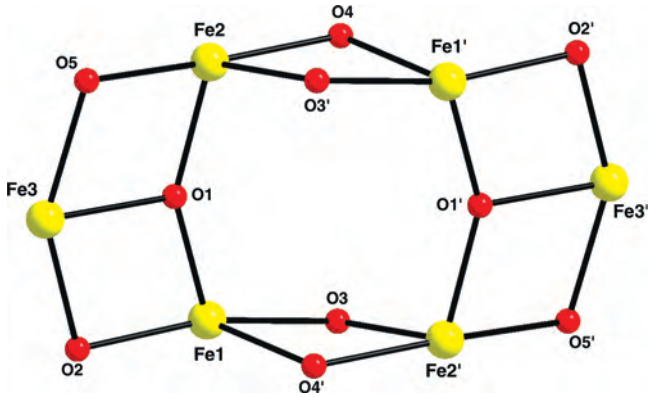

Figure 2. PovRay representation of the labeled core of **1**. Color scheme: Fe, yellow; O, red.

$[Fe_6O_2(hmp)_{10}(H_2O)_2](NO_3)_4$,[6a] and these also have an $S = 3$ ground state. These two complexes are structurally somewhat similar to **1**, differing in the ligation at the end Fe atoms Fe3 and Fe3′: $[Fe_6O_2Cl_4(hmp)_8]^{2+}$ has only two terminal Cl^- ligands at each of these Fe atoms, which are thus five-coordinate, whereas $[Fe_6O_2(hmp)_{10}(H_2O)_2]^{4+}$ has a chelating hmp^- and a terminal water at each of these atoms.

A labeled representation of complex **2** is shown in Figure 3. Selected interatomic distances and angles are given in

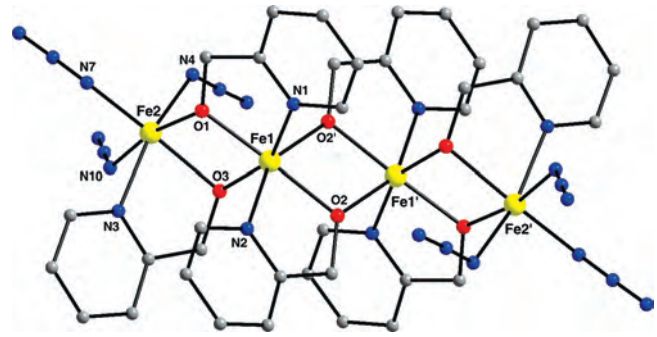

Figure 3. Labeled PovRay representation of the structure of **2**. Hydrogen atoms have been omitted for clarity.

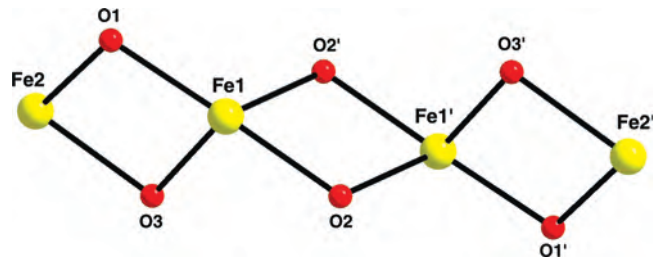

Figure 4. PovRay representation of the labeled core of **2**. Color scheme: Fe, yellow; O, red.

Table 2. Complex **2**·2MeOH crystallizes in the monoclinic space group $P2_1/c$ with the Fe_4 molecule lying on an inversion center. The molecule comprises a nonlinear array of four Fe^{III} atoms (Fe2−Fe1−Fe1′ = 129.73°) with each Fe_2 pair bridged by the alkoxide arms of two chelating hmp^- groups (Figure 4). There is thus a total of six $\eta^1{:}\eta^2{:}\mu$ hmp^- groups, and peripheral ligation is completed by six terminal azide groups, three each on the two end Fe atoms Fe2 and Fe2′. The central Fe(1)−O(2)−Fe(1′)−O(2′) rhomb is strictly planar as a result of the inversion center, and the other two rhombs are nearly so, with the Fe(1)−O(1)−Fe(2)−O(3) torsion angle being 5.2°. The Fe^{III} atoms are both six-coordinate with distorted octahedral geometry, with Fe1 having the greater distortion from ideal geometry. The Fe−N and Fe−O bond lengths are as expected for high-spin iron(III).[42]

There have been a large number of Fe_4 complexes reported in the literature, and these possess a wide variety of metal topologies such as rectangles, rhombs, butterflies, etc.[43] However, the only previous Fe_4 compounds with a similar kind of extended, chain-like topology as in **2** and an

(34) (a) Christmas, C. A.; Tsai, H. L.; Pardi, L.; Kesselman, J. M.; Gantzel, P. K.; Chadha, R. K.; Gatteschi, D.; Harvey, D. F.; Hendrickson, D. N. *J. Am. Chem. Soc.* **1993**, *115*, 12483. (b) Jones, L. F.; Jensen, P.; Moubaraki, B.; Cashion, J. D.; Berry, K. J.; Murray, K. S. *Dalton Trans.* **2005**, 3344. (c) Cañada-Vilalta, C.; Rumberger, E.; Brechin, E. K.; Wernsdorfer, W.; Folting, K.; Davidson, E. R.; Hendrickson, D. N.; Christou, G. *J. Chem. Soc., Dalton Trans.* **2002**, 4005. (d) Yoon, S.; Lippard, S. J. *J. Am. Chem. Soc.* **2005**, *127*, 8386.

(35) (a) Smith, A. A.; Coxall, R. A.; Harrison, A.; Helliwell, M.; Parsons, S.; Winpenny, R. E. P. *Polyhedron.* **2004**, *23*, 1557. (b) Ammala, P. S.; Cashion, J. D.; Kepert, C. M.; Murray, K. S.; Moubaraki, B.; Spiccia, L.; West, B. O. *J. Chem. Soc., Dalton Trans.* **2001**, 2032. (c) Micklitz, W.; Lippard, S. J. *J. Am. Chem. Soc.* **1988**, *27*, 3067. (d) Micklitz, W.; Bott, S. G.; Bentsen, J. G.; Lippard, S. J. *J. Am. Chem. Soc.* **1989**, *111*, 372. (e) Çelenligil-Çetin, R.; Staples, R. J.; Stavropoulos, P. *Inorg. Chem.* **2000**, *39*, 5838.

(36) Christmas, C. A.; Tsai, H. L.; Pardi, L.; Kesselman, J. M.; Gantzel, P. K.; Chadha, R. K.; Gatteschi, D.; Harvey, D. F.; Hendrickson, D. N. *J. Am. Chem. Soc.* **1993**, *115*, 12483.

(37) (a) Schneppensieper, T.; Liehr, G.; van Eldik, R.; Ensling, J.; Gütlich, P. *Inorg. Chem.* **2000**, *39*, 5565. (b) Shweky, I.; Pence, L. E.; Papaefthymiou, G. C.; Sessoli, R.; Yun, J. W.; Bino, A.; Lippard, S. J. *J. Am. Chem. Soc.* **1997**, *119*, 1037. (c) Saalfrank, R. W.; Glaser, H.; Demleitner, B.; Hampel, F.; Chowdhry, M. M.; Schünemann, V.; Trautwein, A. X.; Vaughan, G. B. M.; Yeh, R.; Davis, A. V.; Raymond, K. N *Chem. Eur. J.* **2002**, *8*, 493. (d) Harding, C. J.; Henderson, R. K.; Powell, A. K. *Angew. Chem., Int. Ed.* **1993**, *32*, 570.

(38) (a) Hegetschweiler, K.; Schmalle, H. W.; Streit, H. M.; Gramlich, V.; Hund, H.-U.; Erni, I. *Inorg. Chem.* **1992**, *31*, 1299. (b) Hegetschweiler, K.; Schmalle, H. W.; Streit, H. M.; Schneider, W. *Inorg. Chem.* **1990**, *29*, 3625. (c) Cornia, A.; Gatteschi, D.; Hegetschweiler, K.; Hausherr-Primo, L.; Gramlich, V. *Inorg. Chem.* **1996**, *35*, 4414.

(39) For representative references, see: (a) Burkill, H. A.; Robertson, N.; Vilar, R.; White, A. J. P.; Williams, D. J. *Inorg. Chem.* **2005**, *44*, 3337. (b) Seddon, E. J.; Huffman, J. C.; Christou, G. *J. Chem. Soc., Dalton Trans.* **2000**, 4446. (c) Seddon, E. J.; Yoo, J.; Folting, K.; Huffman, J. C.; Hendrickson, D. N.; Christou, G. *J. Chem. Soc., Dalton Trans.* **2000**, 3640. (d) Nair, V. S.; Hagen, K. S. *Inorg. Chem.* **1992**, *31*, 4048.

(40) (a) Saalfrank, R. W.; Bernt, I.; Chowdhry, M. M.; Hampel, F.; Vaughan, G. B. M. *Chem. Eur. J.* **2001**, *7*, 2765. (b) Murugesu, M.; Abboud, K. A.; Christou, G. *Dalton Trans.* **2003**, 4552. (c) Saalfrank, R. W.; Deutscher, C.; Sperner, S.; Nakajima, T.; Ako, A. M.; Uller, E.; Hampel, F.; Heinemann, F. W. *Inorg. Chem.* **2004**, *43*, 4372. (d) Koizumi, S.; Nihei, M.; Nakano, M.; Oshio, H. *Inorg. Chem.* **2005**, *44*, 1208.

(41) (a) Saalfrank, R. W.; Reimann, U.; Göritz, M.; Hampel, F.; Scheurer, A.; Heinemann, F. W.; Büschel, M.; Daub, J.; Schünemann, V.; Trautwein, A. X. *Chem. Eur. J.* **2002**, *8*, 3614. (b) Tolis, E. I.; Helliwell, M.; Langley, S.; Raftery, J.; Winpenny, R. E. P. *Angew. Chem., Int. Ed.* **2003**, *42*, 3804. (c) Raptopoulou, C. P.; Boudalis, A. K.; Sanakis, Y.; Psycharis, V.; Clemente-Juan, J. M.; Fardis, M.; Diamantopoulos, G.; Papavassiliou, G. *Inorg. Chem.* **2006**, *45*, 2317. (d) Gerbeleu, N. V.; Batsanov, A. S.; Timko, G. A.; Struchkov, Y. T.; Indrichan, K. M.; Popovich, G. A. *Dokl. Akad. Nauk SSSR (Russ.)* **1987**, *293*, 364.

(42) (a) Wemple, M. W.; Coggin, D. K.; Vincent, J. B.; McCusker, J. K.; Streib, W. E.; Huffman, J. C.; Hendrickson, D. N.; Christou, G. *J. Chem. Soc., Dalton Trans.* **1998**, 719. (b) Grant, C. M.; Knapp, M. J.; Huffman, J. C.; Hendrickson, D. N.; Christou, G. *Inorg. Chem.* **1998**, *37*, 6065. (c) Seddon, E. J.; Yoo, J.; Folting, K.; Huffman, J. C.; Hendrickson, D. N.; Christou, G. *J. Chem. Soc., Dalton Trans.* **2000**, 3640.

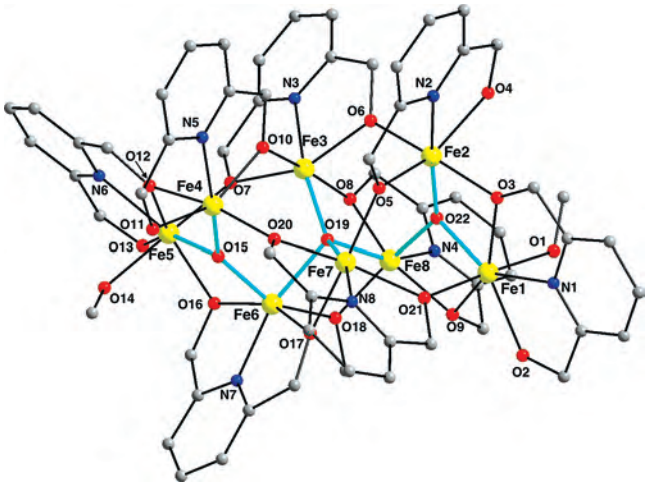

Figure 5. Labeled PovRay representation of the structure of **3**, with the hydrogen atoms omitted for clarity. The core, emphasizing the two Fe_3 triangles and the central Fe_4 tetrahedron, is outlined in cyan. Color code: Fe, yellow; O, red; N, blue; C, gray.

$[Fe_4(\mu\text{-OR})_6]^{6+}$ core are $[Fe_4\{(py)_2C(OMe)O\}_2\{(Hpy)(py)C(OMe)O\}_2(dbcat)_4]^{2+}$[44] (dbcat^{2-} is 3,5-di-t-butylcatecholate) and $[Fe_4(OH)_2(rac\text{-arabitol})_4]^{6-}$.[45]

The partially labeled structure of the $[Fe_8O_3(OMe)(pdm)_4(pdmH)_4(MeOH)_2]^{5+}$ cation of complex **3** is shown in Figure 5. Selected interatomic distances and angles are listed in Table 2. Complex **3** crystallizes in the triclinic space group $P\bar{1}$ with the Fe_8 molecule in a general position. The structure consists of a central $[Fe_4(\mu_4\text{-}O^{2-})]$ tetrahedral subunit (Fe3, Fe6, Fe7, Fe8) fused to two $[Fe_3(\mu_3\text{-}O^{2-})]$ triangular subunits (Fe4, Fe5, Fe6, and Fe1, Fe2, Fe8) at common atoms Fe6 and Fe8 (Figure 6, top). The Fe$-\mu_4$-O$^{2-}-$Fe angles range from 98.1(2) to 131.3(2)°, deviating significantly from the 109.5° ideal values of a tetrahedron. The Fe atoms are additionally bridged by the alkoxide arms of four pdm^{2-} and four pdmH^{-} groups. The pdm^{2-}groups are doubly deprotonated and tridentate-chelating to an Fe atom, with each of their alkoxide arms also bridging to adjacent Fe atoms; these groups are thus $\eta^1{:}\eta^3{:}\eta^1{:}\mu_3$. The pdmH^{-} groups are singly deprotonated and again tridentate-chelating to an Fe atom, but only the deprotonated alkoxide arm bridges to an adjacent Fe atom; these groups are thus $\eta^1{:}\eta^3{:}\mu_3$. In addition, there is a single MeO^{-} group bridging Fe6 and Fe8. The complex therefore contains a $[Fe_8(\mu_4\text{-}O)(\mu_3\text{-}O)_2(\mu\text{-OMe})(\mu\text{-OR})_{12}]$ core (Figure 6, bottom). The ligation is completed by a terminal MeOH group on each of Fe atoms Fe1 and Fe5. The complete cation has only C_1 crystallographic symmetry, but virtual C_2 symmetry, the C_2 axis passing through methoxide O atom O18 and central μ_4-O^{2-} atom O19.

The two $[Fe_3(\mu_3\text{-}O^{2-})]^{7+}$ triangular units are essentially isosceles (Fe1···Fe2 = 3.133(2) Å, Fe1···Fe8 = 3.101(4) Å, Fe2···Fe8 = 3.529(1) Å, and Fe4···Fe5 = 3.129(2) Å, Fe5···Fe6 = 3.094(8) Å, Fe4···Fe6 = 3.541(4) Å), the long separation corresponding to the one not also bridged by a pdm^{2-} or pdmH^{-} alkoxide group. This is also reflected in the geometry at the μ_3-O^{2-} ions, O22 and O15, which have Y-shaped geometry (largest Fe$-$O$-$Fe angles of 138.1(2) and 139.4(2)°, respectively) rather than the trigonal planar geometry usually seen in triangular metal carboxylates;[46] O22 and O15 are also 0.285 and 0.256 Å, respectively, above their Fe_3 planes.

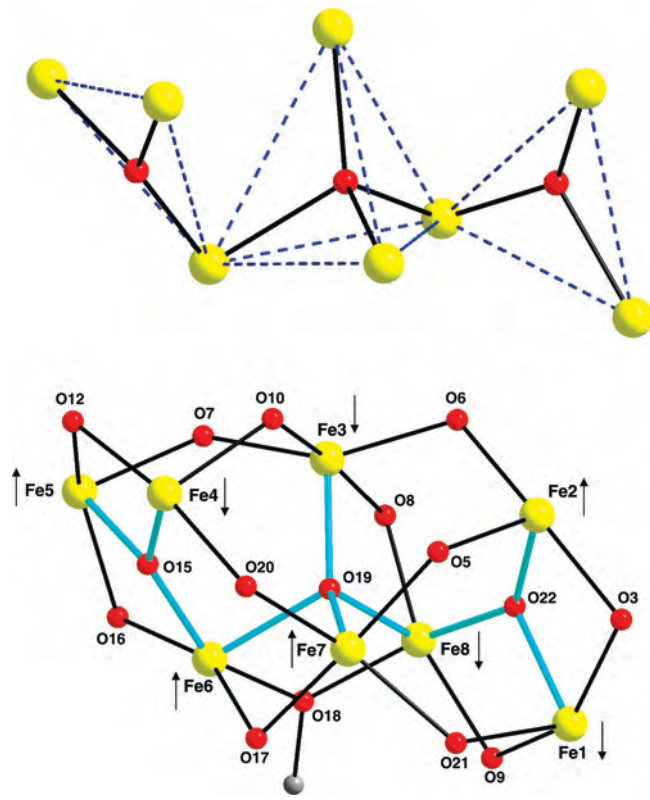

Figure 6. (Top) The Fe_8 topology, emphasizing the triangular $[Fe_3(\mu_3\text{-}O)]^{7+}$ and tetrahedral $[Fe_4(\mu_4\text{-}O)]^{10+}$ subcores (blue dashed lines). (Bottom) PovRay representation of the labeled $[Fe_8O_3(OMe)(OR)_{12}]^{5+}$ core of **3**. Arrows represent spin alignments in the ground state; see the text for discussion. Color scheme: Fe, yellow; O, red; C, grey.

Six of the Fe atoms (Fe2, Fe3, Fe4, Fe6, Fe7, and Fe8) are six-coordinate with distorted octahedral geometries, whereas Fe1 and Fe5 are seven-coordinate with distorted pentagonal bipyramidal geometries. The Fe$-$N and Fe$-$O bond lengths are as expected for high-spin iron(III).[42] As expected, there are H-bonds involving terminal MeOH groups and protonated pdmH^{-} alcohol groups with the lattice MeOH groups and ClO_4^{-} counterions, these interactions serving to link neighboring Fe_8 molecules in the crystal.

Complex **3** joins a small family of cagelike Fe clusters of nuclearity eight. Since most of these were reported only relatively recently, we have listed them in Table 3 for a convenient comparison of their structural type and pertinent magnetic data such as their ground-state spin (*S*) values (vide infra); we have not included in this listing the single-strand

(43) For representative references, see (a) Stamatatos, Th. C.; Christou, A. G.; Jones, C. M.; O'Callaghan, B. J.; Abboud, K. A.; O'Brien, T. A.; Christou, G. *J. Am. Chem. Soc.* **2007**, *129*, 9840. (b) Stamatatos, Th. C.; Boudalis, A. K.; Sanakis, Y.; Raptopoulou, C. P. *Inorg. Chem.* **2006**, *45*, 7372.
(44) Boudalis, A. K.; Dahan, F.; Bousseksou, A.; Tuchagues, J.-P.; Perlepes, S. P. *Dalton Trans.* **2003**, 3411.
(45) Burger, J.; Klüfers, P. *Z. Anorg. Allg. Chem.* **1997**, *623*, 1547.
(46) (a) Cotton, F. A.; Wilkinson, G. *Advanced Inorganic Chemistry*; Wiley: New York, 1980; pp 154−155. (b) Cannon, R. D.; White, R. P. *Prog. Inorg. Chem.* **1988**, *36*, 195.

Table 3. Structural Types and Ground-State S Values for Octanuclear Fe^{III} Clusters

complex[a,b]	core	type	S	ref
$[Fe_8O_4(pz)_{12}Cl_4]$	$[Fe_8(\mu_4\text{-}O)_4]^{16+}$	c	0	47
$[Fe_8O_4(sao)_8(py)_4]$	$[Fe_8(\mu_4\text{-}O)_4]^{16+}$	c	0	48
$[Fe_8O_4(O_2CPh)_{11}(hmp)_5]$	$[Fe_8(\mu_3\text{-}O)_4]^{16+}$	d	0	10
$[Fe_8O_4(O_2CMe)_{12}(hmp)_4]$	$[Fe_8(\mu_3\text{-}O)_4]^{16+}$	d	0	10
$[Fe_8O_4(O_2CPh)_{14}(OR)_2(ROH)_2]$	$[Fe_8(\mu_4\text{-}O)_2(\mu_3\text{-}O)_2]^{16+}$	e	0	12a
$[Fe_8O_4(L)_4Cl_8]$	$[Fe_8(\mu_4\text{-}O)_4]^{16+}$	c	n.r.	49
$[Fe_8O_5(O_2CMe)_8(tren)_4]^{6+}$	$[Fe_8(\mu_4\text{-}O)(\mu_3\text{-}O)_4]^{14+}$	f	n.r.	50
$[Fe_8O_4(OH)_4(Me_2hda)_4(en)_4]$	$[Fe_8(\mu_3\text{-}O)_4(\mu\text{-}OH)_4]^{12+}$	g	0	51
$[Fe_8O_4(OH)_4(O_2CMe)_4(BMDP)_4]^{4+}$	$[Fe_8(\mu\text{-}O)_4(\mu\text{-}OH)_4]^{12+}$	h	n.r.	52
$[Fe_8O_2(OH)_{12}(tacn)_6]^{8+}$	$[Fe_8(\mu_3\text{-}O)_2(\mu\text{-}OH)_{12}]^{8+}$	i	n.r.	53
$[Fe_8O_2(OH)_2(O_2CMe)_2(cit)_6(im)_2]^{8-}$	$[Fe_8(\mu_3\text{-}O)_2(\mu\text{-}OH)_2]^{18+}$	j	0	54
$[Fe_8O_3(O_2CCMe_3)_6(N_3)_3(tea)(teaH)_3]$	$[Fe_8(\mu_4\text{-}O)_3]^{18+}$	k	n.r.	55
$[Fe_8O_3(OMe)(pdm)_4(pdmH)_4(MeOH)_2]^{5+}$ (**3**)	$[Fe_8(\mu_4\text{-}O)(\mu_3\text{-}O)_2]^{18+}$	l	0	t.w.

[a] Counterions and solvate molecules are omitted. [b] Abbreviations: n.r. = not reported; t.w. = this work; pzH = pyrazole; $saoH_2$ = salicylaldehyde oxime; py = pyridine; LH_2 = (2-aminoethyl)-2-hydroxyethyl-(3-hydroxypropyl)amine; tren = tris(2-aminoethyl)amine; Me_2hdaH_3 = *N*-(5-allyl-2-hydroxy-3-methoxybenzyl)iminodiacetic acid; en = ethylenediamine; BMDPH = *N*,*N*,*N*′-tris((*N*-methyl)-2-benzimidazolylmethyl)-*N*′-methyl-1,3-diamino-2-propanol; tacn = 1,4,7-triazacyclononane; $citH_4$ = citric acid; im = imidazole; $teaH_3$ = triethanolamine. Key: c, $[Fe_4(\mu_3\text{-}O)_4]^{4+}$ cube within an Fe_4 tetrahedron; d, four linked $[Fe_3(\mu_3\text{-}O)]^{7+}$ triangles; e, double butterfly; f, four vertex-fused $[Fe_3(\mu_3\text{-}O)]^{7+}$ triangles about a $\mu_4\text{-}O^{2-}$ ion; g, distorted Fe_8 cubane; h, distorted Fe_8 square; i, four Fe about an Fe_4 butterfly; j, two linked Fe_4 tetrahedra; k, three edge-sharing Fe_4 tetrahedra; l, $[Fe_4(\mu_4\text{-}O)]$ tetrahedron fused with two $[Fe_3(\mu_3\text{-}O)]^{7+}$ triangles.

Fe_8 molecular wheel complexes. Examination of Table 3 shows that complex **3** represents a new structural type, as well as being the first homometallic iron(III) cluster with pdm^{2-} and/or $pdmH^-$ groups.

Magnetochemistry

Direct Current Magnetic Susceptibility Studies. Variable-temperature magnetic susceptibility measurements were performed on powdered polycrystalline samples of **1**−**3**, restrained in eicosane to prevent torquing, in a 1 kG (0.1 T) field and in the 5.0–300 K range.

$\chi_M T$ for **1** steadily decreases from 9.79 cm^3 K mol^{-1} at 300 K to a near-plateau value of ∼6.80 cm^3 K mol^{-1} at 50–15 K and then slightly decreases to 6.43 cm^3 K mol^{-1} at 5.0 K (Figure 7). The 300 K value is much less than the spin-only (g = 2) value of 26.25 cm^3 K mol^{-1} for six noninteracting Fe^{III} ions, indicating the presence of strong antiferromagnetic interactions, as expected for oxo-bridged Fe^{III} systems. The 5.0 K value is close to the spin-only (g = 2) value of a complex with an S = 3 ground state (6.00 cm^3 K mol^{-1}). For **2**, $\chi_M T$ steadily decreases from 12.56 cm^3 K mol^{-1} at 300 K to 0.56 cm^3 K mol^{-1} at 5.0 K (Figure 8). Again, the 300 K value is much less than the spin-only (g = 2) value of 17.50 cm^3 K mol^{-1} for four noninteracting Fe^{III} ions, indicating the presence of strong antiferromagnetic exchange interactions and an S = 0 ground state. For complex **3**, $\chi_M T$ decreases steeply from 11.77 cm^3 K mol^{-1} at 300 K to 0.67 cm^3 K mol^{-1} at 5.0 K (Figure 7). The 300 K value is once more much less than the spin-only (g = 2) value of 35.00 cm^3 K mol^{-1} for eight noninteracting Fe^{III}

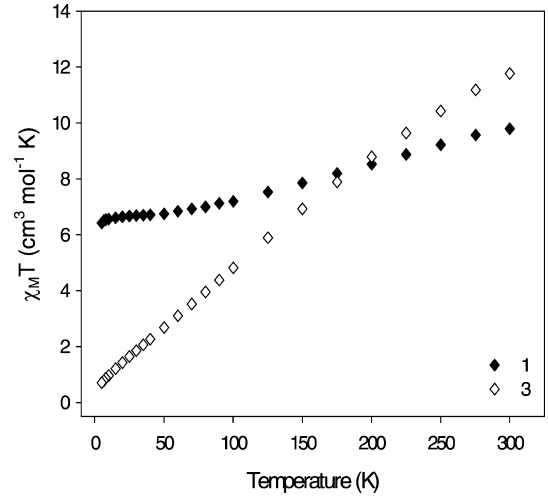

Figure 7. Plots of $\chi_M T$ vs T for complexes **1** and **3**.

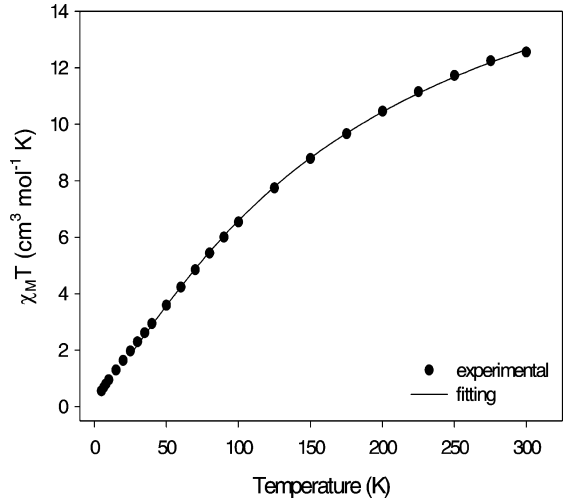

Figure 8. Plot of $\chi_M T$ vs T for complex **2**. The solid line is the fit of the data; see the text for the fit parameters.

(47) Raptis, R. G.; Georgakaki, I. P.; Hockless, D. C. R. *Angew. Chem., Int. Ed.* 1999, *38*, 1632.
(48) Gass, I. A.; Milios, C. J.; Whittaker, A. G.; Fabiani, F. P. A.; Parsons, S.; Murrie, M.; Perlepes, S. P.; Brechin, E. K. *Inorg. Chem.* **2006**, *45*, 5281.
(49) Hahn, F. E.; Jocher, C.; Lugger, T. *Z. Naturforsch. B* **2004**, *59*, 855.
(50) Nair, V. S.; Hagen, K. S. *Inorg. Chem.* **1994**, *33*, 185.
(51) Schmitt, W.; Murugesu, M.; Goodwin, J. C.; Hill, J. P.; Mandel, A.; Bhalla, R.; Anson, C. E.; Heath, S. L.; Powell, A. K. *Polyhedron* **2001**, *20*, 1687.
(52) Satcher, J. H., Jr.; Olmstead, M. M.; Droege, M. W.; Parkin, S. R.; Noll, B. C.; May, L.; Balch, A. L. *Inorg. Chem.* **1998**, *37*, 6751.
(53) Wieghardt, K.; Pohl, K.; Jibril, I.; Huttner, G. *Angew. Chem., Int. Ed. Engl.* **1984**, *23*, 77.
(54) Gautier-Luneau, I.; Fouquard, C.; Merle, C.; Pierre, J.- L.; Luneau, D. *Dalton Trans.* **2001**, 2127.
(55) Ako, A. M.; Waldmann, O.; Mereacre, V.; Klöwer, F.; Hewitt, I. J.; Anson, C. E.; Güdel, H. U.; Powell, A. K. *Inorg. Chem.* **2007**, *46*, 756.

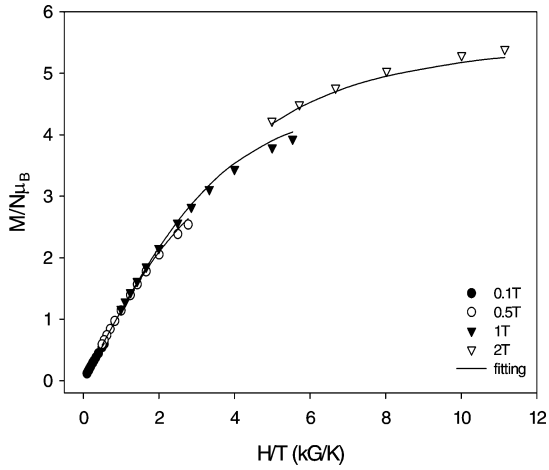

Figure 9. Magnetization (M) vs field (H) and temperature (T) data, plotted as reduced magnetization ($M/N\mu_B$) vs H/T, for complex **1** at applied fields of 0.1−2.0 T and in the 1.8–10 K temperature range. The solid lines are the fit of the data; see the text for the fit parameters.

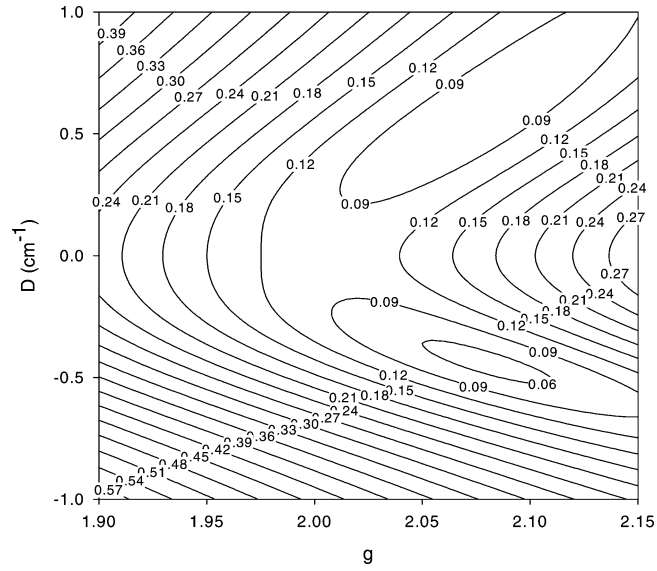

Figure 10. Two-dimensional contour plot of the root-mean-square error surface for the D vs g fit for complex **1**.

ions, indicating the presence of strong antiferromagnetic interactions and an $S = 0$ ground state.

To confirm the indicated $S_T = 3$ ground state of complex **1** and to estimate the magnitude of the zero-field splitting parameter D, magnetization vs dc field measurements were made on restrained samples at applied magnetic fields and temperatures in the 1–70 kG and 1.8–10.0 K ranges, respectively. The resulting data for **1** are shown in Figure 9 as a reduced magnetization ($M/N\mu_B$) *vs* H/T plot, where M is the magnetization, N is Avogadro's number, μ_B is the Bohr magneton, and H is the magnetic field. The data were fit using the program MAGNET[17a] to a model that assumes that only the ground state is populated at these temperatures and magnetic fields, includes isotropic Zeeman interactions and axial zero-field splitting ($D\hat{S}_z^2$) and incorporates a full powder average. The corresponding spin Hamiltonian is given by eq 6, where D is the axial ZFS parameter, $\hat{S}_z$ is the easy-axis spin operator, μ_0 is the vacuum permeability, and H is the applied field. The last term in eq 6 is the Zeeman energy associated with an applied magnetic field. Only data collected at fields up to 20 kG (2 T) were employed in the final fit shown in Figure 9, because satisfactory fits could not be obtained using data collected at higher fields. Such problems are normally an indicator of the complicating presence of low-lying excited states with S greater than that of the ground-state and whose M_S levels thus approach those of the ground state with increasing applied fields. The best fit for **1** is shown as the solid lines in Figure 9 and was obtained with $S = 3$ and either of the two sets of parameters: $g = 2.07$, $D = 0.57$ cm^{-1} and $g = 2.08$, $D = -0.44$ cm^{-1}. Alternative fits with $S = 2$ or 4 were rejected because they gave unreasonable values of g and D. It is common to obtain two acceptable fits of magnetization data for a given S value, one with $D > 0$ and the other with $D < 0$, since magnetization fits are not very sensitive to the sign of D. In order to assess which is the superior fit and also to ensure that the true global minimum had been located, we calculated the root-mean-square D versus g error surface using the program GRID,[17b] which calculates the relative difference between the experimental $M/N\mu_B$ data and those calculated for various combinations of D and g. The error surface, plotted as a two-dimensional contour plot in Figure 10, shows only the two minima with positive and negative D values, with the latter being of superior quality and thus suggesting the true sign of D is negative. However, it would require more sensitive techniques such as EPR spectroscopy or magnetization measurements on oriented single-crystals to confirm this. Note, also, that similarly negative D values have been previously reported for many high-nuclearity Fe^{III} clusters.[7a,12e,f,55]

$$\mathscr{H} = D\hat{S}_z^2 + g\mu_B\mu_0\hat{S}\cdot H \qquad (6)$$

Given the small size of complex **2**, the susceptibility data to 300 K were fit by a matrix diagonalization method described elsewhere[18] to obtain the individual pairwise exchange constants J_{ij} between Fe atoms Fe$_i$ and Fe$_j$. The isotropic Heisenberg spin Hamiltonian that is appropriate for centrosymmetric complex **2** is given in eq 7. Three parameters were employed in the fit: exchange constants J_1 and J_2 for the two outer (Fe1−Fe2 and Fe1′−Fe2′) and one central (Fe1−Fe1′) interactions and the g factor. The next-nearest neighbor interactions J_3 were assumed to be zero, as supported by the theoretical studies (vide infra). A temperature-independent paramagnetism (TIP) term was kept constant at 800×10^{-6} cm^3 K mol^{-1}. The fit (solid line in Figure 8) gave $J_1 = -9.2$ cm^{-1}, $J_2 = -12.5$ cm^{-1}, and $g = 2.079$. Similar values of $J_1 = -4.8$ cm^{-1} and $J_2 = -13.0$ cm^{-1} were reported for $[Fe_4\{(py)_2C(OMe)O\}_2\{(Hpy)(py)C(OMe)O\}_2(dbcat)_4]^{2+}$ (dbcat^{2-} = 3,5-di-*tert*-butylcatecholate), which has a similar core structure to **2**.[44] A more detailed discussion of the J values obtained for **2** is given in the following section describing the theoretical calculations.

$$\mathscr{H} = -2J_1(\hat{S}_1\cdot\hat{S}_2 + \hat{S}_{1'}\cdot\hat{S}_{2'}) - 2J_2(\hat{S}_1\cdot\hat{S}_{1'}) - 2J_3(\hat{S}_1\cdot\hat{S}_{1'} + \hat{S}_2\cdot\hat{S}_{2'}) \qquad (7)$$

As expected, the interactions between the Fe^{III} centers in **2** are strongly antiferromagnetic, resulting in a ground-state

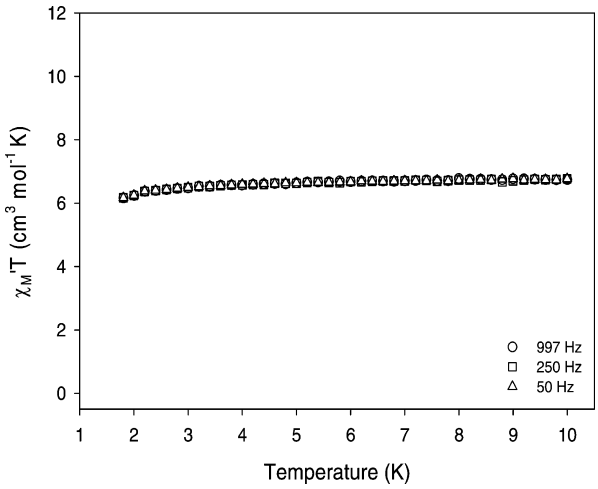

Figure 11. Plot of the in-phase ac susceptibility signals, $\chi'_M T$ vs T for complex **1**.

spin of $S = 0$. The latter is again as expected for a "linear" array of four Fe^{III} atoms, since the constituent exchange interactions J_1 and J_2 are not competing, and $J_3 \approx 0$; thus there are no spin frustration effects in this complex. The theoretical calculations described below confirm this picture and the resultant $S = 0$ ground state (vide infra). Because of the combination of their greater size, complexity, and lower symmetry, the fitting of the experimental susceptibility data for complexes **1** and **3** was not pursued.

Alternating Current Magnetic Susceptibility Studies. As we have described before on multiple occasions, ac susceptibility studies are a powerful complement to dc studies for determining the ground state of a system, because they preclude any complications arising from the presence of a dc field. We thus chose to carry out ac studies on complex **1** as an independent probe of its ground state *S*. These were performed in the 1.8–10 K range using a 3.5 G ac field oscillating at frequencies in the 50–1000 Hz range.

If the magnetization vector can relax fast enough to keep up with the oscillating field, then there is no imaginary (out-of-phase) susceptibility signal (χ''_M), and the real (in-phase) susceptibility (χ'_M) is equal to the dc susceptibility. However, if the barrier to magnetization relaxation is significant compared to thermal energy (kT), then the in-phase signal decreases and a nonzero, frequency-dependent χ''_M signal appears, which is suggestive of the superparamagnetic-like properties of a SMM. For complex **1**, the in-phase $\chi'_M T$ signal below 10 K is almost temperature independent (Figure 11), and extrapolation of the plot to 0 K from above 3 K (to avoid dips at the lowest T due to anisotropy, weak intermolecular interactions, etc.) gives a value of ~6.4 cm^3 K mol^{-1} range. This indicates an $S = 3$ ground state and $g \sim 2.07$, in excellent agreement with the dc magnetization fit. Finally, complex **1** did not exhibit an out-of-phase ac magnetic susceptibility signal down to 1.8 K, indicating that it does not exhibit a barrier large enough vs kT, down to 1.8 K at least, to show the superparamagnet-like slow relaxation of its magnetization vector, i.e., it is not a SMM. Studies at much lower temperatures would be required to search for what would at best be a tiny relaxation barrier.

Complex **1** is thus confirmed to possess an $S = 3$ ground state, which is a most unusual ground state for an Fe^{III}_6 complex. Most of the Fe^{III}_6 complexes for which the ground-state spin has been determined have an $S = 0$ or $S = 5$ ground state. In fact, it is not intuitively obvious how an $S = 3$ ground state could arise in **1**, since it is clearly not the resultant of simple considerations of spin-up and spin-down alignment pictures. The usual qualitative rationalization in such cases is to say that spin frustration effects must be operative within the Fe_3 triangular subunits, with spin frustration defined as in the Introduction. Thus, a qualitative argument would say that intermediate spin alignments ($M_S = \pm 3/2, \pm 1/2$ for high-spin Fe^{III}) are present at some or all of the Fe atoms, and this gives the observed $S = 3$ ground state. A more satisfying quantitative computational treatment is clearly needed. As mentioned earlier, the structurally related complex $[Fe_6O_2Cl_4(hmp)_8](ClO_4)_2$ was also found to have an $S = 3$ ground state;[36] attempts to quantitatively explain it by computational methods unfortunately proved inconclusive, the calculations predicting an $S = 0$ ground state. Thus, we have recently undertaken and are in the midst of a detailed, quantitative analysis of the exchange interactions, degree of spin frustration as a function of exact symmetry, and resulting spin alignments in Fe^{III}_6 complexes with the structure of **1** but have chosen for this analysis the related complex $[Fe_6O_2(hmp)_{10}(H_2O)_2](NO_3)_4$ with $S = 3$.[6a] We thus postpone further discussion of the magnetic properties of these unusual $S = 3$ complexes to the detailed full paper to follow. In the present paper, we shall instead provide a detailed, quantitative analysis by computational methods of the exchange interactions in complexes **2** and **3**, which will provide a rationalization of their observed $S = 0$ ground states.

Theoretical Studies. In order to provide independent estimates of the constituent exchange constants, theoretical calculations were carried out on complex **2** with DFT and on complexes **2** and **3** with the semiempirical ZILSH method.[18,19] For complex **2**, the spin Hamiltonian of eq 7 was assumed with three exchange parameters: J_1 and J_2 for the outer (Fe1−Fe2 and Fe1′−Fe2′) and central (Fe1−Fe1′) interactions, respectively, and J_3 for next-nearest-neighbor (Fe1−Fe2′ and Fe1′−Fe2) interactions. Together with E_0, there are thus four parameters to be determined in eq 1, requiring calculations on four spin components. The components used were the "high-spin" (HS) component with all unpaired spins aligned parallel, and those with unpaired spins on Fe1 and Fe1′, Fe1 and Fe2, or Fe1 and Fe2′ reversed, i.e. aligned antiparallel to all other unpaired spins.

Energies were computed for these components with ZILSH and DFT (B3LYP functional,[25] LANL2DZ basis set[26,27]), while spin couplings were computed from the ZILSH wave functions. Results for the high-spin component are presented in Table 4 along with spin densities computed for each metal atom with both methods. Similar results are given for all components considered as Supporting Information (Table S1). The spin densities are close to the formal value of five expected for high-spin d^5 Fe^{3+} ions but are reduced below this number by spin delocalization, as found with ZILSH

Table 4. Computational Results for High-Spin Components of **2** and **3**[a]

quantity	complex **2**		complex **3**	
E (ZILSH)	1458.8[b,c]		5349.9[d,e]	
E (DFT)	905.7[b,c]			
local spin densities	M_1[f]	4.34 (4.12)	M_1[g]	4.38
	M_2	4.18 (3.96)	M_2	4.38
	M_1'	4.34 (4.12)	M_3	4.40
	M_2'	4.18 (3.96)	M_4	4.38
			M_5	4.38
			M_6	4.36
			M_7	4.40
			M_8	4.34

[a] See text for discussion and descriptions of methods and basis sets used. [b] Energy of high-spin component of **2** relative to energy of component with spins of Fe1 and Fe2′ reversed relative to those of Fe1′ and Fe2 (cm^{-1}). See Figure 4 for numbering scheme. [c] Absolute energy of HS component (a.u.): −631.19465008 from ZILSH; −3651.58831273 from DFT. [d] Energy of high-spin component of **3** relative to energy of component with spins of Fe2 and Fe4 reversed relative to all others (cm^{-1}). See Figure 6 for numbering scheme. [e] Absolute energy of HS component (a.u.) is −1035.45169076 (ZILSH method). [f] Component of spin for Fe1 of **2** from ZILSH calculations. See Figure 4 for numbering scheme. Values in parentheses were obtained from DFT calculations. [g] Component of spin for Fe1 of **3** from ZILSH calculations. See Figure 6 for numbering scheme.

for other complexes of Fe^{3+} ions.[18,19,30,31] Values obtained with DFT calculations are similar to the ZILSH values and resemble those reported for similar calculations.[56,57] The signs of the local spin densities indicate the relative directions of spin moments of the iron ions, and demonstrate that correct spin distributions were obtained for each spin component with both methods. Spin couplings $\langle \hat{S}_A \cdot \hat{S}_B \rangle^{UHF}$ found from ZILSH wave functions with the local spin operator also have values close to ±5, similar to those obtained from ZILSH calculations on other polynuclear Fe^{3+} complexes.[18,19,30,31]

Examination of the energies found for each component (Table 4) shows that the HS component was the one calculated by both methods to have the highest energy, indicating that the exchange interactions in **2** are predominantly antiferromagnetic. The component with unpaired spins on Fe1 and Fe2′ reversed relative to the unpaired spins on Fe1′ and Fe2 (see Figure 4) was found to have the lowest energy with both methods, as expected for a linear core with antiferromagnetic interactions. Exchange constants obtained from the energies and spin couplings found for **2** (see Table S1 in Supporting Information) are presented in Table 5, along with those found from fitting the magnetic susceptibility data of the complex (vide supra). All methods indicate that the exchange interactions J_1 and J_2 are antiferromagnetic, with J_2 for the central Fe1−Fe1′ interaction slightly stronger than J_1 for the outer Fe1−Fe2 and Fe1′−Fe2′ interactions. The relative magnitudes of J_1 and J_2 follow the magnetostructural correlations established for oxo-bridged ferric complexes,[18,58–60] with larger antiferromagnetic interactions associated with shorter Fe−O bond distances and larger Fe−O−Fe angles (average bond distances and angles: 1.993 Å, 105.2° and 2.018 Å, 103.5° for the J_2 and J_1 pathways, respectively). The next-nearest-neighbor interaction J_3 was found to be essentially zero with both computational methods. Both methods overestimate the magnitudes of J_1 and J_2, with DFT performing significantly better than ZILSH for these interactions. The opposite was found for both hydroxide- and oxide-bridged interactions in $[Fe_8O_2(OH)_{12}(tacn)_6]^{8+}$.[31] Additional comparative studies of the methods are needed to judge if one method is consistently more accurate than the other or under what conditions (e.g., type of bridging ligands, pathway geometries) one outperforms the other.

An additional factor to consider is that the model employed in the calculations just described for **2** included assumptions regarding the symmetry of the complex and the strength and equivalency of certain exchange interactions, e.g., neglecting the third neighbor Fe2−Fe2′ interaction, assuming equivalent Fe1−Fe2 and Fe1′−Fe2′ interactions (J_1 in Table 5). A more general procedure is to consider enough components to solve for all pairwise exchange constants without such assumptions, and in the past this has been the approach we have used. Given that DFT calculations have sometimes shown the tendency to overestimate second neighbor interactions (e.g., DFT calculations on Fe_4 butterfly complexes that gave exchange constants on the order of -10 cm^{-1} for second neighbor "wingtip−wingtip" interactions[57]), we performed DFT calculations on additional components to see if the assumptions used above had any effect on the results obtained. Energies and spin couplings were computed for seven components of **2** (see Table S4 in Supporting Information), allowing all pairwise exchange constants to be obtained by simultaneous solution of eq 1. These calculations gave, in the numbering scheme of Figure 4, $J_{12} = J_{1'2'} = -15.3$ cm^{-1} in exact agreement with J_1 of Table 5. Also $J_{11'} = -18.8$ cm^{-1} was obtained, in agreement with J_2 of Table 5. All other interactions, including both second neighbor interactions $J_{12'}$ and $J_{1'2}$ (J_3 in Table 5) and the third neighbor $J_{22'}$ interaction, were found to be 0.1 cm^{-1} or less in magnitude. These DFT calculations thus displayed no tendency to overestimate exchange interactions between metals that are not directly bridged.

Calculations were performed on complex **3** with the ZILSH method, but not with DFT because of the large size and low symmetry of the complex. Owing to the latter, 29 spin components were considered so that all pairwise exchange constants in the complex could be solved for independently. The components used were the high-spin HS component, and all unique components in which the unpaired spins on two metal ions were reversed (antiparallel) relative to all others (i.e., spins of Fe1 and Fe2 reversed, spins of Fe1 and Fe3 reversed, etc.). Calculated energies and local spin densities for the high-spin component are given in Table 4. Similar results for all 29 components are given as Supporting Information (Table S2). Again, the HS component is substantially higher in energy than the other components, indicating the presence of antiferromagnetic interactions in the complex. The spin densities are close to the formal value of five expected for high-spin d^5 Fe^{3+} ions but are reduced below this number by spin delocalization, as found with ZILSH for **2** (Table 4) and other complexes of

(56) Ruiz, E.; Cano, J.; Alvarez, S. *Chem. Eur. J.* **2005**, *11*, 4767.
(57) Cauchy, T.; Ruiz, E.; Alvarez, S. *J. Am. Chem. Soc.* **2006**, *128*, 15722.
(58) Gorun, S. M.; Lippard, S. J. *Inorg. Chem.* **1991**, *30*, 1625.
(59) Weihe, H.; Güdel, H. U. *J. Am. Chem. Soc.* **1997**, *119*, 6539.
(60) Werner, R.; Ostrovsky, S.; Griesar, K.; Haase, W. *Inorg. Chim. Acta* **2001**, *326*, 78.

Table 5. Exchange Constants Determined by Various Methods and Relevant Structural Intracore Details for Complex **2**

interaction[a]	ZILSH	DFT	FIT[b]	av Fe−OR distances (Å)	av Fe−OR−Fe angles (deg)	type of bridge
J_1	−24.2	−15.3	−9.2	2.018	103.5	μ-OR$^-$
J_2	−31.2	−18.8	−12.5	1.993	105.2	μ-OR$^-$
J_3	0.2	0.0	(0.0)	long magnetic pathway	long magnetic pathway	long magnetic pathway

[a] Units in cm^{-1}. [b] Values obtained from fitting of the magnetic susceptibility data. See text for details.

Table 6. Nonzero Exchange Constants Calculated for Complex **3** with ZILSH, Associated Spin Couplings $\langle \hat{S}_A \cdot \hat{S}_B \rangle$ Computed for the Ground State Spin Wavefunction, and Relevant Structural Intracore Details

interaction[a]	J (cm^{-1})	$\langle \hat{S}_A \cdot \hat{S}_B \rangle$[b]	av Fe−OR distances (Å)	av Fe−OR−Fe angles (deg)	type of bridges
J_{12}	−42.6	−6.66	1.981	100.3	μ_3-O^{2-}, μ-OR$^-$
J_{17}	−19.5	−7.26	2.049	126.3	μ-OR$^-$
J_{18}	−20.4	5.62	2.021	100.5	μ_3-O^{2-}, μ-OR$^-$
J_{23}	−16.7	−5.12	2.040	118.1	μ-OR$^-$
J_{27}	−17.3	5.24	2.008	117.1	μ-OR$^-$
J_{28}	−62.0	−7.84	1.890	138.1	μ_3-O^{2-}
J_{34}	−16.8	5.35	2.009	117.0	μ-OR$^-$
J_{35}	−18.7	−7.21	2.053	125.2	μ-OR$^-$
J_{36}	−12.9	−5.24	2.024	112.5	μ_4-O^{2-}
J_{37}	−24.6	−7.45	1.955	131.3	μ_4-O^{2-}
J_{38}	−14.4	4.92	2.028	99.3	μ_4-O^{2-}, μ-OR$^-$
J_{45}	−44.5	−6.77	1.975	105.0	μ_3-O^{2-}, μ-OR$^-$
J_{46}	−63.6	−7.79	1.888	139.4	μ_3-O^{2-}
J_{47}	−17.7	−5.15	2.029	118.3	μ-OR$^-$
J_{56}	−19.5	5.72	2.015	100.6	μ_3-O^{2-}, μ-OR$^-$
J_{67}	−15.2	4.96	2.022	98.9	μ_4-O^{2-}, μ-OR$^-$
J_{68}	−10.4	−6.30	2.033	102.3	μ_4-O^{2-}, μ-OMe$^-$
J_{78}	−12.9	−5.05	2.024	112.5	μ_4-O^{2-}

[a] $-2J$ convention; see Figure 6 for numbering scheme. [b] Spin couplings computed from the ground-state spin eigenfunction obtained by substituting the exchange constants into the Heisenberg Hamiltonian and diagonalizing in a basis of spin components. See the Theoretical Methods section for details.

Fe^{3+} ions.[18,19,30,31] The signs of the local spin densities indicate the relative directions of spin moments of the iron ions and demonstrate that correct spin distributions were obtained for each spin component. The spin couplings $\langle \hat{S}_A \cdot \hat{S}_B \rangle^{UHF}$ found from ZILSH wave functions with the local spin operator (given as Supporting Information due to their large number, Table S3) also have values close to ±5, similar to those obtained from ZILSH calculations on other polynuclear Fe^{3+} complexes.[18,19,30,31]

Nonzero exchange constants obtained from the data of Tables S2 and S3 are presented in Table 6. The various interactions are indicated using the numbering scheme of Figure 6. Focusing first on interactions within the triangular subunits of the Fe_8 core (i.e., Fe1, Fe2, Fe8; Fe4, Fe5, Fe6), they approximately follow the virtual C_2 symmetry of the complex and so are similar for the two sets of ions; discussion is thus limited to the Fe1−Fe2−Fe8 unit. The J_{28} pathway is bridged by a μ_3-O^{2-} ligand, while the J_{12} and J_{18} pathways are bridged by μ_3-O^{2-} and μ-OR$^-$ ligands. Oxide-mediated interactions are generally much stronger than alkoxide-mediated interactions,[58] so oxide-mediated interactions can be expected to make the dominant contribution to J_{12} and J_{18}. The values found for the three interactions again follow established correlations between larger magnitude and both shorter Fe−O bond distances and larger Fe−O−Fe angles in the oxide-mediated pathways[18,58–60] ($J_{28} = -62.0$ cm^{-1}, Fe−O−Fe angle 138.1°, average Fe−O distance 1.89 Å; $J_{12} = -42.6$ cm^{-1}, angle 109.2°, average distance 1.92 Å; $J_{18} = -20.4$ cm^{-1}, 105.6°, 1.95 Å).

Interactions within the central Fe_4 subunit (Fe3, Fe6, Fe7, Fe8) are mediated by the central μ_4-O^{2-} ion and additional alkoxide moieties. For the most part, the oxide-bridged pathways have smaller bond angles and longer bond distances than in the triangular subunits, and the exchange constants are correspondingly smaller in magnitude. The exception to this is the Fe3−μ_4-O^{2-}−Fe7 pathway, with $J_{37} = -24.6$ cm^{-1}, Fe−O−Fe angle 131.3°, average Fe−O distance 1.96 Å. This pathway thus has a substantially larger bond angle than the Fe1−μ_3-O^{2-}−Fe2 pathway, but a substantially smaller exchange constant. This can be attributed to the longer average bond distance (1.96 Å vs 1.92 Å; bond distance is known to have a larger effect than angle[18,60]) and the general observation that coupling through an oxide weakens as the number of metals it bridges increases. Finally, there are additional nonzero exchange interactions between ions in the triangular and tetrahedral subunits. These interactions are generally small in magnitude, as expected since they are mediated by alkoxide bridging ligands only.

The spin alignments giving rise to the diamagnetic ground state of **3** (see Figure 7 and accompanying discussion, vide supra) are not obvious due to the large number of nonzero exchange constants with similar magnitudes in the complex. It is clear that spin frustration is likely taking place in some of the exchange pathways, given the large number of triangular motifs in the core structure (Figure 6). That being the case, even the spin of the ground state predicted by the calculations is unclear when considering the exchange constants of Table 6. Spin eigenstate calculations were therefore carried out to determine the ground-state spin and gain a more detailed picture of spin alignments in the complex. These calculations show that the ground state has $S = 0$ and is stabilized relative to the $S = 1$ first excited state by 25.4 cm^{-1}. Spin alignments in an $S = 0$ ground state are difficult to describe because the z components of spin average to zero due to equally weighted contributions to the state wavefunction of spin components with reversed spin moments. For example, the leading contributions to the $S = 0$ ground state of **3** are made by the spin components

$$\left|\frac{5}{2},-\frac{5}{2},\frac{5}{2},\frac{5}{2},-\frac{5}{2},-\frac{5}{2},-\frac{5}{2},\frac{5}{2}\right\rangle$$

and

$$\left|-\frac{5}{2},\frac{5}{2},-\frac{5}{2},-\frac{5}{2},\frac{5}{2},\frac{5}{2},\frac{5}{2},-\frac{5}{2}\right\rangle$$

In such cases it is useful to consider the spin couplings $\langle \hat{S}_A \cdot \hat{S}_B \rangle$ computed from the ground-state wavefunction,

which provide a direct probe of spin frustration: if J_{AB} and $\langle \hat{S}_A \cdot \hat{S}_B \rangle$ carry different signs, the A−B pathway is frustrated.[30,31] Spin couplings are presented in Table 6 and show that the J_{18}, J_{27}, J_{34}, J_{38}, J_{56}, and J_{67} pathways are frustrated. Considering Figure 6, then, the most weakly coupled pathways in the two Fe_3 subunits of the core are frustrated, as expected for a triangular arrangement of coupled spins. Two of the weaker pathways in the Fe_4 subunit are frustrated, along with two of the interactions between subunits. All interactions are antiferromagnetic, so the z components of spin of the metals in the frustrated pathways align parallel in all spin components contributing to the ground-state wavefunction, as seen in the two spin components listed above. This suggests spin alignments as depicted by the arrows in Figure 6. It should be noted that these arrows are not meant to imply nonzero z components of spin for the metal ions but rather the relative directions of the z components in each spin component contributing to the ground-state wavefunction.

Conclusions

The bidentate N,O and tridentate O,N,O ligands hmp^- and $pdm^{2-}/pdmH^-$ in noncarboxylate Fe^{III} chemistry have proven to be a useful route to new Fe^{III} clusters spanning Fe_4, Fe_6, and Fe_8 nuclearities and topologies that are either very rare or prototypical. In particular, the reaction between $Fe(NO_3)_3 \cdot 9H_2O$ and hmpH in basic media has led to $[Fe_6O_2(NO_3)_4(hmp)_8(H_2O)_2](NO_3)_2$ (**1**), whereas the same reaction but with the addition of NaN_3 gives the tetranuclear cluster $[Fe_4(N_3)_6(hmp)_6]$ (**2**). It is interesting that the azide ligands in **2** are terminal rather than bridging but, nevertheless, fostered formation of a product completely different from that of the nonazide product **1**. Similarly, replacement of hmpH with $pdmH_2$ gave the novel cluster $[Fe_8O_3(OMe)(pdm)_4(pdmH)_4(MeOH)_2]^{5+}$ (**3**).

The ground states and constituent exchange constants of complexes **2** and **3** were determined by DFT and/or ZILSH theoretical methods. Those for **2** were computed by both methods, and this allowed a useful comparison of the methods and their agreement with the experimentally determined J values from magnetization fits. Both methods gave good agreement with the overall conclusions of the analysis of experimental data, in terms of the ground states of the complex and the sign and relative magnitude of the constituent J values, although the latter from DFT did agree better with the experimentally determined J values. It is becoming apparent that sometimes DFT gives the more "accurate" numbers (as gauged by comparisons with experimental fits) and sometimes ZILSH does. However, the added advantage of ZILSH in conveniently handling higher nuclearity complexes was emphasized by its ready application to Fe_8 complex **3**. It correctly predicted the experimentally observed $S = 0$ ground state and also rationalized it by identifying the pattern of spin frustration effects occurring within its many Fe_3 triangular subunits. This convenient, quantitative explanation of why and how this complicated molecule is $S = 0$ is a further reflection of the power of the ZILSH approach.

Acknowledgment. This work was supported by NSF (CHE-0414555 to G.C.) and an IBM Shared University Research grant to IU (T.O'B.). C.M.J. and K.M.P. acknowledge funding from the Undergraduate Research Opportunities Program at IUPUI.

Supporting Information Available: X-ray crystallographic files in CIF format for complexes **1**·6MeCN, **2**·2MeOH, and **3**·7MeOH, computational results for spin components of **2** (Table S1) and **3** (Table S2), spin couplings computed from ZILSH wave functions for spin components of **3** (Table S3), and computational results for additional spin components of **2** (Table S4). This material is available free of charge via the Internet at http://pubs.acs.org.

IC701756P